Fluxional η^3-Allyl Derivatives of *ansa*-Scandocenes and an *ansa*-Yttrocene. Measurements of the Barriers for the η^3 to η^1 Process as an Indicator of Olefin Binding Energy to d^0 Metallocenes

Michael B. Abrams, Jeffrey C. Yoder, Cyrille Loeber, Michael W. Day, and John E. Bercaw*

Arnold and Mabel Beckman Laboratories of Chemical Synthesis, California Institute of Technology, Pasadena, California 91125

Received October 30, 1998

Variable-temperature ^{1}H NMR spectroscopy indicates fluxional behavior for a number of group 3 metallocene allyl complexes. Spectral simulations and line shape analyses for the variable-temperature spectra indicate an allyl rearrangement mechanism involving rate-determining carbon−carbon double-bond dissociation from the metal center, *i.e.* an η^3 to η^1 change in coordination. Activation barriers to olefin dissociation have been determined for (η^5-C_5Me_5)$_2$Sc(η^3-C_3H_5), *meso*-Me_2Si(η^5-3-CMe_3-C_5H_3)$_2$Sc(η^3-C_3H_5), *meso*-Me_2Si[η^5-2,4-$(CHMe_2)_2$-C_5H_2]$_2$Sc(η^3-C_3H_5), *meso*-Me_2Si\{η^5-3-[2-(2-Me)-adamantyl]-C_5H_3\}$_2$Sc(η^3-C_3H_5), *meso*-Me_2Si-\{η^5-3-[2-(2-Me)-adamantyl]-C_5H_3\}$_2$Y(η^3-C_3H_5), *rac*-Me_2Si[η^5-2,4-$(CHMe_2)_2$-C_5H_2]$_2$Sc(η^3-C_3H_5)), and *R*-($C_{20}H_{12}O_2$)Si(η^5-2-$SiMe_3$-4-CMe_3-C_5H_2)$_2$Sc(η^3-C_3H_5): $\Delta G^{\ddagger} = 11-16$ kcal mol^{-1} at *ca.* 300−350 K. Donor solvents do not significantly affect the rate of olefin dissociation. A second rearrangement mechanism that involves 180° rotation of the η^3-C_3H_5 moiety has been found to operate in those metallocenes whose ancillary ligand arrays adopt rigid meso geometries. Line shape analysis indicates that the rate of η^3-C_3H_5 rotation is generally more than 1 order of magnitude faster than olefin dissociation for a given meso metallocene. The data do not allow unambiguous assessments of the mechanism(s) for the fluxional behavior for the allyl derivatives of the racemic metallocenes. An X-ray structure determination for *rac*-Me_2Si[η^5-C_5H_2-2,4-$(CHMe_2)_2$]$_2$Sc(η^3-C_3H_5) has been carried out.

Introduction

Organometallic complexes incorporating the allyl ligand are known for almost every transition metal.[1] Two bonding modes for the allyl ligand are well-established: η^3-C_3H_5 and η^1-C_3H_5. The η^3-C_3H_5 mode is much more common, especially for middle[2] and late[3] transition metals, where metal to allyl back-bonding is strong. Moreover, the η^3-C_3H_5 mode is favored even for early-transition-metal[4] and lanthanide and actinide[5] metals in high formal valencies, where metal to allyl back-bonding is expected to be relatively weak. Particularly for this last class of complexes, the allyl ligand commonly exhibits fluxional behavior associated with

(1) Collman, J. P.; Hegedus, L. S.; Norton, J. R.; Finke, R. G. *Principles and Applications of Organotransition Metal Chemistry*; University Science Books: Mill Valley, CA, 1987.

(2) (a) Van Baalen, A.; Groenenboom, C. J.; De Liefde Meijer, H. J. *J. Organomet. Chem.* **1974**, *74*, 245. (b) Siegert, F. W.; De Liefde Meijer, H. J. *J. Organomet. Chem.* **1970**, *23*, 177. (c) Gibson, V. C.; Parkin, G.; Bercaw, J. E. *Organometallics* **1991**, *10*, 220. (d) Doherty, N. M. Ph.D. Thesis, California Institute of Technology, 1984. (e) Cheatham, L. K.; Graham, J. J.; Apblett, A. W.; Barron, A. R. *Polyhedron* **1991**, *10*, 1075. (f) Faller, J. W.; Chen, C.-C.; Mattina, M. J.; Jakubowski, A. *J. Organomet. Chem.* **1973**, *52*, 361. (g) Cotton, F. A.; Marks, T. J. *J. Am. Chem. Soc.* **1969**, *91*, 1339. (h) Trofimenko, S. *Inorg. Chem.* **1970**, *9*, 2493. (i) Holloway, C. E.; Kelly, J. D.; Stiddard, M. H. B. *J. Chem. Soc. A* **1969**, 931.

(3) (a) Faller, J. W.; Adams, M. A. *J. Organomet. Chem.* **1979**, *170*, 71. (b) Fish, R. W.; Giering, W. P.; Marten, D.; Rosenblum, M. *J. Organomet. Chem.* **1976**, *105*, 101. (c) Vrieze, K. In *Dynamic Nuclear Magnetic Resonance Spectroscopy*; Jackman, L. M., Cotton, F. A., Eds.; Academic Press: New York, 1975; p 44. (d) Jolly, P. W.; Mynott, R. *Adv. Organomet. Chem.* **1981**, *19*, 257. (e) Vrieze, K.; Cossee, P.; Praat, A. P.; Hilbers, C. W. *J. Organomet. Chem.* **1968**, *11*, 353. (f) Vrieze, K.; Volger, H. C. *J. Organomet. Chem.* **1967**, *9*, 537. (g) Volger, H. C.; Vrieze, K. *J. Organomet. Chem.* **1967**, *9*, 527. (h) Cotton, F. A.; Faller, J. W.; Musco, A. *Inorg. Chem.* **1967**, *6*, 179.

(4) (a) Thompson, M. E.; Baxter, S. M.; Bulls, A. R.; Burger, B. J.; Nolan, M. C.; Santarsiero, B. D.; Schaefer, W. P.; Bercaw, J. E. *J. Am. Chem. Soc.* **1987**, *109*, 203. (b) Bunel, E.; Burger, B. J.; Bercaw, J. E. *J. Am. Chem. Soc.* **1988**, *110*, 976. (c) Martin, H. A.; Jellinek, F. *J. Organomet. Chem.* **1968**, *12*, 149. (d) Vance, P. J.; Prins, T. J.; Hauger, B. E.; Silver, M. E.; Wemple, M. E.; Pederson, L. M.; Kort, D. A.; Kannisto, M. R.; Geerlings, S. J.; Kelly, R. S.; McCandless, J. J.; Huffman, J. C.; Peters, D. G. *Organometallics* **1991**, *10*, 917. (e) Tjaden, E. B.; Casty, G. L.; Stryker, J. M. *J. Am. Chem. Soc.* **1993**, *115*, 9814. (f) Chen, J.; Kai, Y.; Kasai, N.; Yasuda, H.; Yamamoto, H.; Nakamura, A. *J. Organomet. Chem.* **1991**, *407*, 191. (g) Helmholdt, R. B.; Jellinek, F.; Martin, H. A.; Vos, A. *Recl. Trav. Chim. Pays-Bas* **1967**, *86*, 1263. (h) Dick, D. G.; Duchateau, R.; Edema, J. J. H.; Gambarotta, S. *Inorg. Chem.* **1993**, *32*, 1959. (i) Larson, E. J.; Van Dort, P. C.; Lakanen, J. R.; O'Neill, D. W.; Pederson, L. M.; McCandless, J. J.; Silver, M. E.; Russo, S. O.; Huffman, J. C. *Organometallics* **1988**, *7*, 1183. (j) Larson, E. J.; Van Dort, P. C.; Dailey, J. S.; Lakanen, J. R.; Pederson, L. M.; Silver, M. E.; Huffman, J. C.; Russo, S. O. *Organometallics* **1987**, *6*, 2141. (k) Horton, A. D. *Organometallics* **1992**, *11*, 3271. (l) Antonelli, D. M.; Tjaden, E. B.; Stryker, J. M. *Organometallics* **1994**, *13*, 763. (m) Jordan, R. F.; LaPointe, R. E.; Bradley, P. K.; Baenziger, N. *Organometallics* **1989**, *8*, 2892. (n) Krieger, J. K.; Deutch, J. M.; Whitesides, G. M. *Inorg. Chem.* **1973**, *12*, 1535. (o) Landis, C. R.; Cleveland, T.; Casey, C. P. *Inorg. Chem.* **1995**, *34*, 1285. (p) Benn, R.; Rufinska, A.; Schroth, G. *J. Organomet. Chem.* **1981**, *217*, 91. (q) Arewgoda, M.; Rieger, P. H.; Robinson, B. H.; Simpson, J.; Visco, S. T. *J. Am. Chem. Soc.* **1982**, *104*, 5633. (r) Tjaden, E. B.; Stryker, J. M. *J. Am. Chem. Soc.* **1993**, *115*, 2083. (s) Hauger, B. E.; Vance, P. J.; Prins, T. J.; Wemple, M. E.; Kort, D. A.; Silver, M. E.; Huffman, J. C. *Inorg. Chim. Acta* **1991**, *187*, 91. (t) Prins, T. J.; Hauger, B. E.; Vance, P. J.; Wemple, M. E.; Kort, D. A.; O'Brien, J. P.; Silver, M. E.; Huffman, J. C. *Organometallics* **1991**, *10*, 979. (u) Jaitner, P.; Wohlgennant, W.; Gieren, A.; Betz, H.; Hubner, T. *J. Organomet. Chem.* **1985**, *297*, 281. (v) Becconsall, J. K.; Job, B. E.; O'Brien, S. *J. Chem. Soc. A* **1967**, 423.

10.1021/om980893s CCC: $18.00
Publication on Web 03/13/1999

Scheme 1

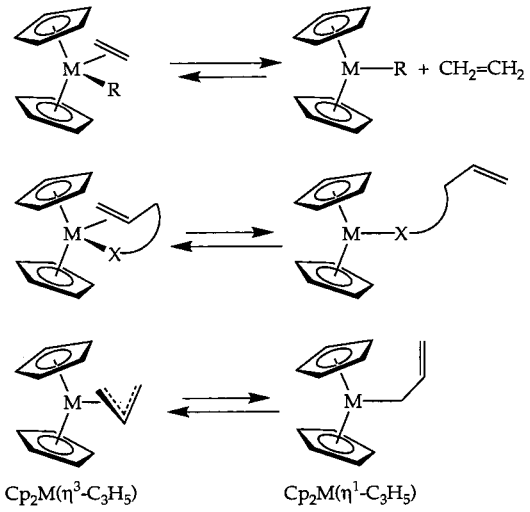

allyl rotation and/or η^3-$C_3H_5 \rightleftarrows \eta^1$-$C_3H_5$ interconversions, and the mechanistic aspects of these processes have been investigated for almost three decades.

Olefin adducts of d^0 metallocenes are currently of great interest due to their proposed intermediacy in Ziegler−Natta olefin polymerizations.[6] Jordan[7] and Casey[8] have recently reported examples of moderately stable olefin adducts of such d^0 metallocenes, $[(\eta^5\text{-}C_5H_5)_2Zr(\eta^1(O):\eta^2\text{-}OCMe_2CH_2CH_2CH{=}CH_2)]^+$ and $(\eta^5\text{-}C_5Me_5)_2Y(\eta^1{:}\eta^2\text{-}CH_2CH_2CMe_2CH{=}CH_2)$. Royo has very recently reported another type of intramolecular coordination of an olefin to a zirconocene cation, one for which the olefin is tethered to a cyclopentadienyl ligand: $[(\eta^5\text{-}C_5H_5)(\eta^7\text{-}C_5H_4SiMe_2CH_2CH{=}CH_2)Zr(CH_2C_6H_5)][B(C_6F_5)_4]$.[9] The strength of the metal−olefin interaction appears to be too small to allow isolation of an olefin adduct without chelation. It occurred to us that η^3-C_3H_5 derivatives represent common examples, albeit special cases, of such chelated olefin adducts of d^0 metallocenes (Scheme 1). Moreover, the barrier for η^3 to η^1 conversion is an upper limit for the strength of the olefin−metal interaction.

Several examples of formally d^0 metallocene allyl complexes have been reported. Although the barriers for η^3-$C_3H_5 \rightleftarrows \eta^1$-$C_3H_5$ interconversions generally have not been established, there are some unusual and poorly understood qualitative differences among seemingly closely related allyl complexes.[10] Some complexes are firmly η^3-coordinated; *e.g.*, $(\eta^5\text{-}C_5Me_5)_2Ln(\eta^3\text{-}C_3H_5)$ (Ln = La, Nd, Sm) are nonfluxional on the ^{1}H NMR time scale at 25 °C in hydrocarbon solvents (the neodymium complex is static on the magnetization transfer time scale at +90 °C).[5b] On the other hand, $(\eta^5\text{-}C_5Me_5)_2Sm(\eta^3\text{-}C_3H_5)$ is fluxional at 25 °C in THF solution, and $(\eta^5\text{-}C_5Me_5)_2Sm(\eta^3\text{-}C_3H_4\text{-}1\text{-}CH_3)$ is fluxional even at −80 °C.[5a,c] $(\eta^5\text{-}C_5Me_5)_2Sc(\eta^3\text{-}C_3H_5)$ requires cooling below 0 °C to obtain the spectrum for the static structure, in hydrocarbon solvents.[4a] Isoelectronic cationic group 4 metallocenium cations also display both static and fluxional NMR character; *e.g.*, $[(\eta^5\text{-}C_5Me_5)_2Ti(\eta^3\text{-}C_3H_5)]^+$ is reported to be static at −18 °C, but the zirconium analogue is fluxional at 25 °C in toluene-d_8 and nearly static at −78 °C in methylene chloride-d_2.[4l,r] In contrast, $[(\eta^5\text{-}C_5Me_5)_2Zr(\eta^3\text{-}C_3H_5)(CO)]^+$ is static at 25 °C in methylene chloride-d_2.[4l] Neutral cyclopentadienyl−aminoborole analogues to the metallocene allyls $(\eta^5\text{-}C_5Me_5)[\eta^5\text{-}C_4H_4BN(CHMe_2)_2]M(\eta^3\text{-}C_3H_5)$ (M = Zr, Hf) are static even at 80 °C, but the closed-shell, 18-electron adducts $(\eta^5\text{-}C_5Me_5)[\eta^5\text{-}C_4H_4BN(CHMe_2)_2]M(\eta^3\text{-}C_3H_5)(L)$ (M = Zr, Hf; L = PMe_3, THF, methylimidazole) are fluxional at 25 °C.[11] The carbonyl adduct $(\eta^5\text{-}C_5Me_5)[\eta^5\text{-}C_4H_4BN(CHMe_2)_2]Hf(\eta^3\text{-}C_3H_5)(CO)$ undergoes very slow rotation about the Hf−$(\eta^3\text{-}C_3H_5)$ bond (*vide infra*).[11] Thus, it is difficult to fully reconcile the factors which promote fluxional allyl behavior for these formally d^0 metallocene allyl compounds.[12]

While fluxional behavior has been noted for allyl complexes of d^0 metallocenes, there appear to have been no studies that have established the mechanisms for fluxionality. Complicating the assessment of the barrier for $\eta^3 \rightarrow \eta^1$ interconversion is the fact that more than one mechanism may be contributing to dynamic behavior. The two most widely accepted unimolecular mechanisms for explaining the observed spectroscopic behavior of metal(η^3-allyl) complexes are (Scheme 2) (1) a stepwise process involving dissociation of the allyl C=C double bond, rotation about the allyl C−C single bond, and recoordination of the C=C double bond to regenerate η^3 coordination[4a,p,v] and (2) η^3-C_3H_5 rotation,[2f,5c,4n,p] which involves a 180° rotation of the η^3-coordinated ligand about an axis perpendicular to the C−C−C plane.

NMR spectroscopy employing magnetization transfer experiments or line shape analysis has proven invaluable in studies of such processes for late- and middle-transition-metal allyl complexes. Fluxional allyl behavior is generally identified by observing the exchange between *syn* and *anti* substituents on the allyl moiety and/or the exchange between two types of *syn* and two types of *anti* sites (if they are inequivalent in the static structure). Since both rotation about the M−allyl bond and dissociation of the C=C double bond may disrupt the π bonding for the η^3-coordinated allyl, those allyl complexes that are prone to undergo rapid $\eta^3 \rightleftarrows \eta^1$ shifts also might be expected to undergo rotation. Thus, care must be taken in interpreting dynamic NMR behavior. It is therefore not surprising that the information concerning the dynamics of allyl complexes of metallocenes generally has been only qualitative.

Only two complexes reported previously, the monomeric, homoleptic allyls $Mo(\eta^3\text{-}C_3H_5)_4$ and $W(\eta^3\text{-}C_3H_5)_4$, have been unambiguously shown to undergo both (1)

(5) (a) Tsutsui, M.; Ely, N. *J. Am. Chem. Soc.* **1975**, *97*, 3551. (b) Jeske, G.; Lauke, H.; Mauermann, H.; Swepston, P. N.; Schumann, H.; Marks, T. J. *J. Am. Chem. Soc.* **1985**, *107*, 8091. (c) Evans, W. J.; Ulibarri, T. A.; Ziller, J. W. *J. Am. Chem. Soc.* **1990**, *112*, 2314. (d) Hsu, C.-Y.; Orchin, M. *J. Am. Chem. Soc.* **1975**, *97*, 3551. (e) Brunelli, M.; Poggio, S.; Pedritti, U.; Lugli, G. *Inorg. Chim. Acta* **1987**, *131*, 281.

(6) Brintzinger, H. H.; Fischer, D.; Mülhaupt, R.; Rieger, B.; Waymouth, R. N. *Angew. Chem., Int. Ed. Engl.* **1995**, *34*, 1143.

(7) Wu, Z.; Jordan, R. F.; Petersen, J. L. *J. Am. Chem. Soc.* **1995**, *117*, 5867.

(8) (a) Casey, C. P.; Hallenbeck, S. L.; Pollock, D. W.; Landis, C. L. *J. Am. Chem. Soc.* **1995**, *117*, 9770. (b) Casey, C. P.; Hallenbeck, S. L.; Wright, J. M.; Landis, C. R. *J. Am. Chem. Soc.* **1997**, *119*, 9680. (c) Casey, C. P.; Fagan, M. A.; Hallenbeck, S. L. *Organometallics* **1998**, *17*, 287.

(9) Galakhov, M. V.; Heinz, G.; Royo, P. *Chem. Commun.* **1998**, 17.

(10) Moreover, in many cases for which these complexes are fluxional, their assignment as η^3 coordinated, although likely, has not been unambiguously established.

(11) Pastor, A.; Kiely, A. F.; Henling, L. M.; Day, M. W.; Bercaw, J. E. *J. Organomet. Chem.* **1997**, *528*, 65.

(12) Stryker has argued that coordination of carbon monoxide to a d^0 metallocene allyl complex induces strong $\sigma \rightarrow \pi^*$ donation from the neighboring allyl ligand, inhibiting fluxionality in the allyl fragment.

Scheme 2

1. *Syn* ↔ *anti* interconversion by $\eta^3 \rightarrow \eta^1$ / C- C 180° bond rotation / $\eta^1 \rightarrow \eta^3$:

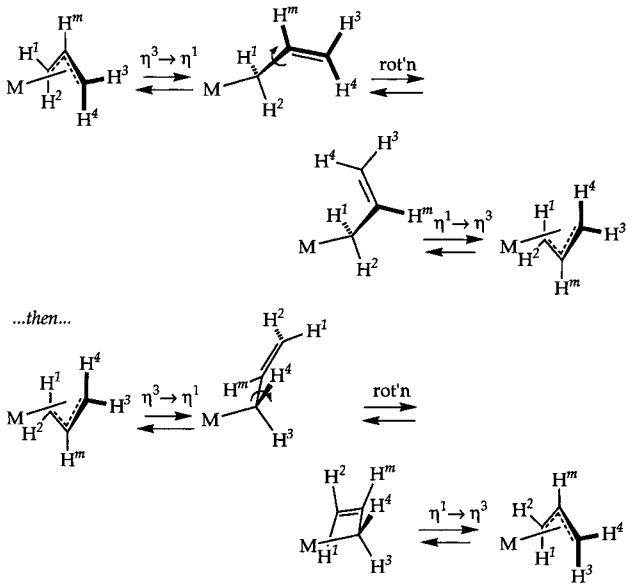

2. Allyl 180° rotation while η^3-coordinated:

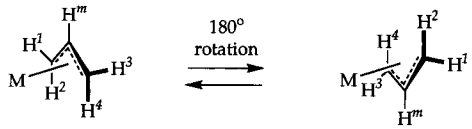

$\eta^3 \rightleftarrows \eta^1$ interconversion and (2) (η^3-C_3H_5) rotation. Magnetization transfer experiments indicate that process 1 is faster than process 2 for Mo(η^3-C_3H_5)$_4$, and although both exchange processes are believed to occur for W(η^3-C_3H_5)$_4$, no rate data for either (1) or (2) has been reported.[4p] Assuming that the ground-state structure of the related Zr(η^3-C_3H_5)$_4$ is the same as that of the molybdenum and tungsten compounds, then both mechanisms 1 and 2 operate in the Zr system; although the slow exchange limit is not observed (−90 °C), η^3-C_3H_5 rotation is the faster of the two processes.[4n,o]

Our research group has been investigating alkyl and hydride derivatives of scandocene and yttrocene, particularly their reactivities toward C−H bonds of hydrocarbons and as neutral, single-component models for cationic, group 4 metallocene olefin polymerization catalysts.[13] The preparation of 14-electron, monomeric species normally requires a very bulky alkyl such as $CH(SiMe_3)_2$ to prevent the formation of oligomers with 3-center, 2-electron bridges, M(μ_2-R)$_2$M. More recently, we have found that conversion of dihalide−scandate or −yttrate derivatives to η^3-allyl complexes, which are subsequently treated with H_2 to afford the hydride derivative, is a convenient alternative synthetic route in some cases (Scheme 3).[14] During the course of these investigations, we have noted that all of the allyl complexes are fluxional. We report in this article mechanistic investigations of the fluxional behavior of several of these allyl complexes.

Scheme 3

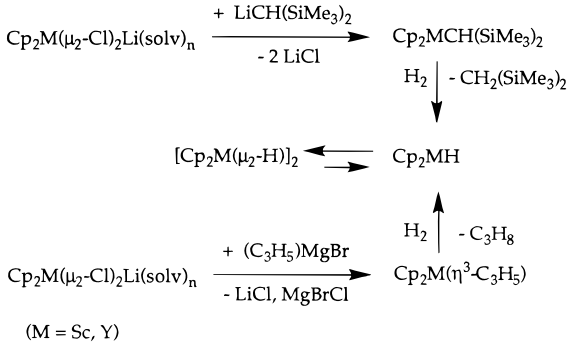

Results and Discussion

Preparation of Allyl Complexes. The bis(cyclopentadienyl)M(η^3-C_3H_5) derivatives examined here are of three basic types (Chart 1): (a) C_s-symmetric (η^5-C_5Me_5)$_2$Sc(η^3-C_3H_5) (**1**),[4a] for which the allyl is coordinated to a C_{2v} symmetric metallocene fragment, (b) C_1-symmetric complexes (**2**, **3**,[15] **4**, **5**) for which the allyl is coordinated to a C_s-symmetric, meso metallocene fragment, and (c) C_1-symmetric complexes (**6**[15] and **7**), for which the allyl is coordinated to C_2-symmetric, racemic (or enantiopure) metallocene fragments.

Chart 1

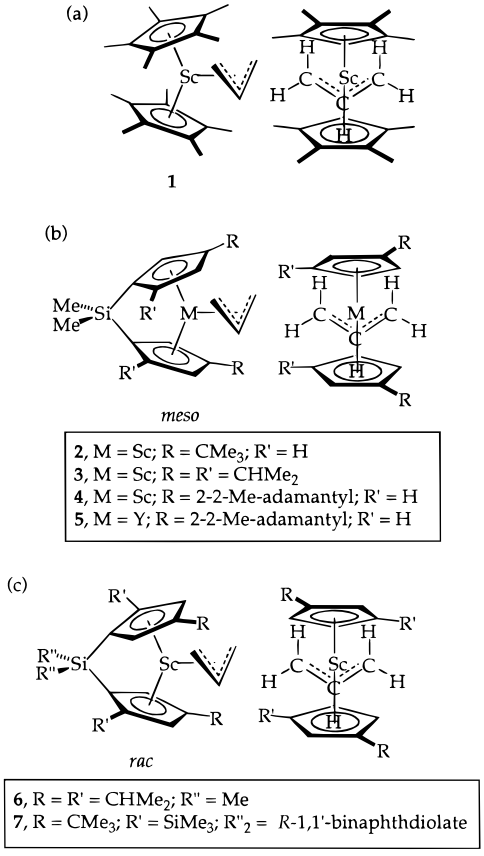

Preparation of {$Me_2Si(\eta^5$-3-CMe_3-$C_5H_3)_2$}Sc(η^3-C_3H_5) (**2**) is performed analogously to that for (η^5-C_5Me_5)$_2$Sc(η^3-C_3H_5) (**1**),[4a] by reaction of the hydride derivative with excess allene (eq 1).

(13) See, for example; (a) Reference 4a. (b) Piers, W. E.; Shapiro, P. J.; Bunel, E. E.; Bercaw, J. E. *Synlett* **1990**, 74. (c) Mitchell, J. P.; Hajela, S.; Brookhart, S. K.; Hardcastle, K. I.; Henling, L. M.; Bercaw, J. E. *J. Am. Chem. Soc.* **1996**, *118*, 1045.

(14) A recent report describing the formation of lanthanocene hydrides by addition of H_2 to η^3-allyl complexes has appeared: Evans, W. J.; Seibel, C. A.; Ziller, J. W. *J. Am. Chem. Soc.* **1998**, *120*, 6745.

(15) Yoder, J. C.; Day, M. D.; Bercaw, J. E. *Organometallics* **1998**, *17*, 4946.

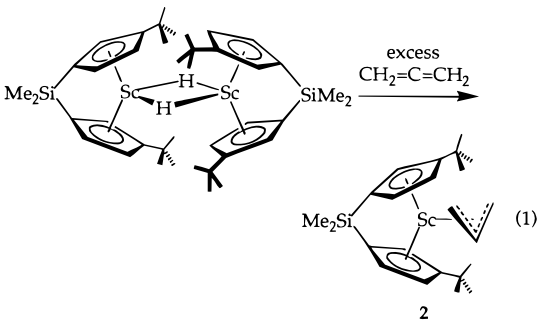

The synthesis of $Li_2[Me_2Si\{3\text{-}[2\text{-}(2\text{-Me})\text{-adamantyl}]\text{-}C_5H_3\}_2]$ is carried out analogously to that for the related ligand $Li_2[Me_2Si(3\text{-}CMe_3\text{-}C_5H_3)_2]$ (Scheme 4).[4b] Hence,

Scheme 4

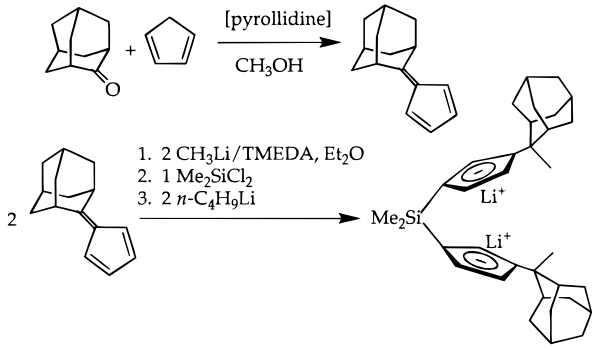

the 6,6′-disubstituted fulvene is treated with methyllithium to generate lithio-2-(2-Me)-adamantylcyclopentadienide, which is isolated as a white solid. This reaction proceeds in the absence of *N*,*N*,*N*′,*N*′-tetramethylethylenediamine (TMEDA), although the TMEDA adduct is preferred for the subsequent linking reaction. Treatment with 0.5 equiv of Me_2SiCl_2 affords $Me_2Si\{3\text{-}[2\text{-}(2\text{-Me})\text{-adamantyl}]\text{-}C_5H_4\}_2$, which is doubly deprotonated using *n*-butyllithium to yield $Li_2[Me_2Si\{3\text{-}[2\text{-}(2\text{-Me})\text{-adamantyl}]\text{-}C_5H_3\}_2]$ as a white powder. Typical overall yields of the four-step synthesis are on the order of 35−40%.

Transmetalations of $Li_2[Me_2Si\{3\text{-}[2\text{-}(2\text{-Me})\text{-adamantyl}]\text{-}C_5H_3\}_2]$ with either $ScCl_3(THF)_3$ or $YCl_3(THF)_{3.5}$ afford the *meso*-$\{Me_2Si\{3\text{-}[2\text{-}(2\text{-Me})\text{-adamantyl}]\text{-}C_5H_3\}_2\}$-$MCl{\cdot}LiCl(THF)_2$ adducts (eq 2). The *meso*-metallocene

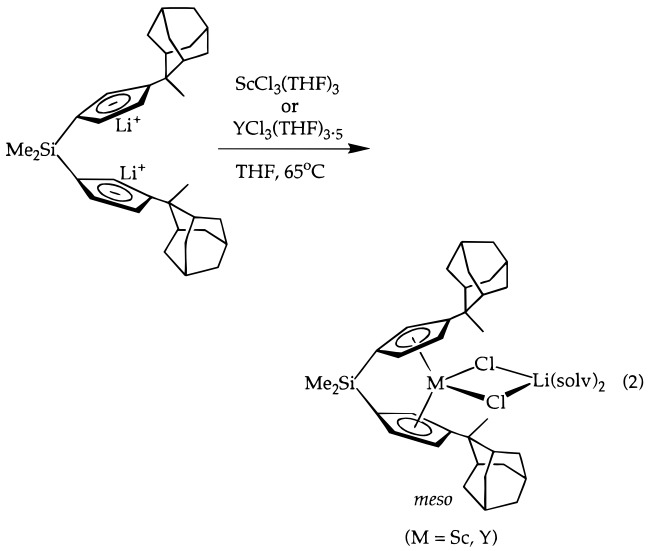

chlorides are formed exclusively, as evidenced by the ^1H NMR spectra of the crude product mixtures. The solvent coordinated to the lithium ions of *meso*-$\{Me_2Si\{\eta^5\text{-}3\text{-}[2\text{-}(2\text{-Me})\text{-adamantyl}]\text{-}C_5H_3\}_2\}M(\mu_2\text{-}Cl)_2Li(solv)_2$ may be varied. For example, THF may be replaced by diethyl ether by a series of diethyl ether and toluene washes.

Treatment with allylmagnesium bromide, beginning at −78 °C and slowly warming to 25 °C, proceeds smoothly for either solvate (eq 3).

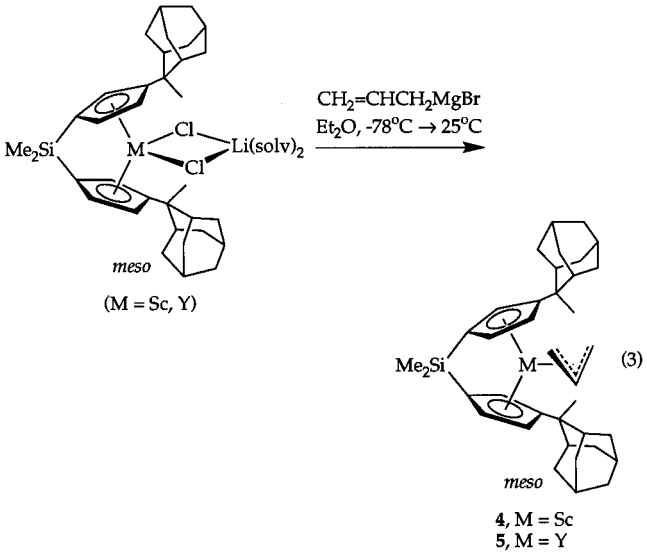

Because **4** and **5** are extremely soluble in both hydrocarbon solvents (toluene, benzene, cyclohexane, pentane) and ether solvents (tetrahydrofuran, diethyl ether) and slightly soluble in hexamethyldisiloxane, neither slow cooling of concentrated solutions nor repeated attempts at crystal growth by vapor diffusion have yielded single crystals suitable for X-ray diffraction studies. Moreover, **4** and **5** appear to retain small amounts (generally less than 1.0 equiv) of the last solvent with which they were in contact, as evidenced by the characteristic resonances in the ^1H NMR of these species. Residual toluene and even petroleum ether are not removed even by prolonged heating under dynamic vacuum. Hence, the elemental analyses of these complexes are generally poor. We assume that the molecules pack only loosely in the crystalline form, perhaps as a result of the 2-(2-methyl)adamantyl substituents, and that solvent molecules are tightly occluded in the pores.

The racemic isomers are obtained using procedures analogous to those that proved successful for **1**−**5**. Thus, treatment of *rac*-$Me_2Si[\eta^5\text{-}2,4\text{-}(CHMe_2)_2\text{-}C_5H_2]_2Sc(\mu_2\text{-}Cl)_2$-$Li(THF)_2$ with a slight excess of allylmagnesium bromide in toluene solution, with slow warming from −78 °C to room temperature, affords **6** in good yield. It is important to carry out this reaction at low temperatures to minimize interconversion of *rac* and *meso* diastereomers.[14]

The optically pure ligand derived from (*R*)-2,2′-binaphthol, *e.g.* $\{((R)\text{-}OC_{10}H_6C_{10}H_6O)Si(C_5H_2\text{-}2\text{-}SiMe_3\text{-}4\text{-}CMe_3)_2\}^{2-}$ ([(*R*)-BnBp]$^{2-}$), has been designed to coordinate to yttrium to produce enantiomerically pure metallocene.[13c] The transmetalation of this ligand with $ScCl_3(THF)_3$ in THF proceeds in a similar manner to yield enantiomerically pure (*R*,*S*)-BnBpScCl(THF).[14] The THF adduct may be converted to [(*R*,*S*)-BnBpSc-

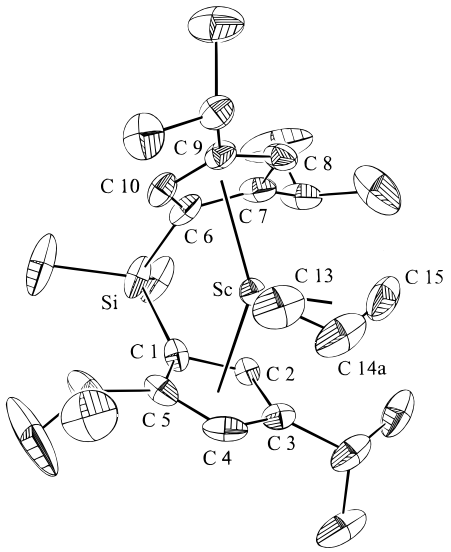

Figure 1. Molecular structure of the molecule of **6** with the major orientation shown (50% probability ellipsoids; hydrogens omitted for clarity). Selected bond distances (Å) and angles (deg) are as follows: Sc−centroid1(C1−C5) = 2.188(1), Sc−centroid2(C6−C10) = 2.189(1), Sc−centroid3A-(C13−C14A−C15, major rotamer) = 2.245(1), Sc−centroid-3B(C13−C14B−C15, minor rotamer) = 2.237(1), Sc−C13 = 2.487(3), Sc−C14A = 2.465(5), Sc−C14B = 2.436(7), Sc−C15 = 2.469(3), C13−C14A = 1.340(8), C14A−C15 = 1.381-(9) Å; centroid1−Sc−centroid2 = 128.5(2), centroid1−Sc−centroid3A = 111.4(1), centroid2−Sc−centroid3A = 120.1(1), C13−C14A−C15 = 128.5(7), C13−Sc−C15 = 59.28(14).

(μ-Cl)]$_2$ by prolonged drying under dynamic vacuum at 120 °C. A molecular weight determination in benzene-d_6 using the Signer technique confirms its dimeric structure in solution. As for the other allyl complexes, reaction with equimolar amounts of allylmagnesium bromide in toluene, again beginning at low temperature and warming the reaction mixture slowly to room temperature, affords the monomeric allyl complex (*R,S*)-BnBp-Sc(η^3-C_3H_5) (**7**). This extremely air- and moisture-sensitive allyl compound is obtained as a red-orange solid by filtration from *n*-hexane. Although once isolated it is practically insoluble in hexane and pentane, the presence of traces of solvents such as toluene and diethyl ether during the workup of the reaction mixture dramatically enhances its solubility in hydrocarbon solvents.

X-ray Structure Determination for *rac*-$Me_2Si[\eta^5$-2,4-$(CHMe_2)_2$-$C_5H_2]_2Sc(\eta^3$-$C_3H_5)$ (6). Upon slow cooling from 80 °C, single crystals of **6** precipitated as orange plates from a saturated toluene solution. Although the allyl ligand is disordered with the methine carbon directed both up and down in the crystal lattice, this disorder was modeled successfully as a 70:30 population of sites, using two separate allyl methine carbons (C(14A) and C(14B)) each directed at one of the cyclopentadienyl rings. The positions of allyl methylene carbons C(13) and C(15) were identical in both molecules. The structure of the molecule oriented in the major position is shown in Figure 1. Details of the data collection and solution and refinement of the structure can be found in Table 1.

The geometry about scandium is probably best described by considering the bonds from scandium to the centroid of each ligand. It is then evident that the scandium is coordinated in an approximately trigonal-planar geometry with the Cp centroid−Sc−Cp centroid angle being 128.5(2)° and the two Cp centroid−Sc−allyl centroid angles slightly less than 120°. For each allyl site the sum of the centroid−Sc−centroid angles is 360°, indicating that the metal center and all three centroids are coplanar. The Sc−Cp centroid bond lengths (2.188-(1) Å and 2.189(1) Å) are identical (within experimental error) and are in the normal range for Sc−Cp bond lengths in scandocene alkyls (2.170−2.212 Å).[4a,16] The Cp centroid−Sc−Cp centroid angle is in excellent agreement with the same angle (128.1°) of the only other crystallographically characterized *ansa*-scandocene alkyl compound, {$Me_2Si(\eta^5$-$C_5Me_4)[\eta^5$-3-$CH_2CH_2P(CMe_3)_2$-$C_5H_3]$}$ScCH(SiMe_3)_2$.[15a]

The allyl ligands in each site appear to be symmetrically bonded η^3-allyl structures. The Sc−C(13) and Sc−C(15) bond lengths of 2.487(3) and 2.469(3) Å, respectively, are only slightly greater than 3σ apart, and the C−C bond lengths in each allyl site are equivalent within standard deviation. Thus, there appears to be no distortion toward an η^1 structure for **6** in the solid state. The bond lengths from scandium to the central allyl methine carbons of each site are slightly shorter than the corresponding scandium−methylene carbon distances: Sc−C(14A) = 2.465(5) Å and Sc−C(14B) = 2.436 (7) Å.

Variable-Temperature ^{1}H NMR Spectra for Allyl Complexes. Rate constants and free energies of activation obtained from the variable-temperature ^{1}H NMR spectra for allyl complexes **1**−**5** are given in Table 2. All of the temperature-dependent changes are reversible; cooling the samples after recording higher temperature spectra results in regeneration of the previously

Table 1. X-ray Diffraction Data Collection Parameters for *rac*-$Me_2Si[\eta^5$-C_5H_2-2,4-$(CHMe_2)_2]_2$-$Sc(\eta^3$-$C_3H_5)$ (6)[a]

empirical formula	$C_{27}H_{43}ScSi$
fw	440.66
cryst size (mm)	0.3 × 0.2 × 0.2
temp (K)	160
space group	$P2_1/c$
cell constants	
a (Å)	13.669(3)
b (Å)	10.601(2)
c (Å)	18.057(4)
β (deg)	92.90(3)
V (Å^3)	2613.2(10)
Z	4
d(calcd) (g/mL)	1.120
2θ range (deg)	4.50−50.00
index ranges	$-16 \le h \le 16$, $-12 \le k \le 12$, $0 \le l \le 21$
no. of rflns collected	10 116
no. of indep rflns	4588
R(merge)	0.0285
GOF(merge)	1.08
no. of data/restraints/params	4583/0/364
GOF(F^2)[b]	2.153
R indices (all data)[c,d]	R1 = 0.0643, wR2 = 0.0950

[a] The structure was obtained on an Enraf-Nonius CAD-4 using Mo Kα radiation (λ = 0.710 73 Å). [b] GOF = $[\sum w(F_o^2 - F_c^2)^2/(n-p)]^{1/2}$ (n = number of data, p = number of variables). [c] R1 = $\sum||F_o| - |F_c||/\sum|F_o|$. [d] wR2 = $\{\sum[w(F_o^2 - F_c^2)^2]/\sum[wF_o^4]\}^{1/2}$.

(16) (a) Schaefer, W. P.; Köhn, R.; Bercaw, J. E. *Acta Crystallogr.* **1992**, *C48*, 251. (b) Hajela, S.; Schaefer, W. P.; Bercaw, J. E. *Acta Crystallogr.* **1992**, *C48*, 1771. (c) St. Clair, M.; Schaefer, W. P.; Bercaw, J. E. *Organometallics* **1991**, *10*, 525. (d) Campion, B. K.; Heyn, R. H.; Tilley, T. D. *Organometallics* **1993**, *12*, 2584.

Table 2. Summary of Rates and Activation Free Energies for $\eta^3 \rightarrow \eta^1$ Allyl Conversion (k_1, $\Delta G_1^{\ddagger}$) and for η^3-C_3H_5 Rotation (k_2, $\Delta G_2^{\ddagger}$) for Allyl Complexes of Meso Metallocenes 2−5, As Estimated from gNMR Simulations

complex	solvent	T (K)	k_1 (s^{-1})	k_2 (s^{-1})	$\Delta G_1^{\ddagger}(T)$ (kcal mol^{-1})	$\Delta G_2^{\ddagger}(T)$[a] (kcal mol^{-1})
2	toluene-d_8	246		70		12.2
2	toluene-d_8	327	7800		13.4	
3	toluene-d_8	259		490		11.9
3	toluene-d_8	362	7600		14.9	
4	Et_2O-d_{10}	207	6.5	260	11.2	9.7
4	Et_2O-d_{10}	246	260	20000	11.6	9.5
4	Et_2O-d_{10}	290	5200		12.0	
5	Et_2O-d_{10}	208		110		10.1
5	Et_2O-d_{10}	361	2800		15.6	
5	toluene-d_8	370	2800		16.0	

[a] Uncertainty in the free energies of activation are estimated to be approximately ±1.0 kcal mol^{-1}.

observed lower temperature spectra, although prolonged heating at temperatures above 60 °C does lead to decomposition.

In toluene-d_8 solution (η^5-C_5Me_5)$_2$Sc(η^3-C_3H_5) (**1**) displays an AM_2X_2 pattern ($^3J_{syn-m} = 5$ Hz; $^3J_{anti-m} = 15$ Hz) for the allyl protons and inequivalent η^5-C_5Me_5 resonances at the two lowest temperatures examined, 194 K at 500 MHz and 210 K at 300 MHz, as expected for the static structure. The small (unresolvable) geminal coupling observed for formally d^0 **1** contrasts with the considerable geminal $^2J_{H-H}$ value of 7.6 Hz observed for the closely related (η^5-C_5Me_5)$_2$Ta(η^3-C_3H_5).[2c] Moreover, the smaller difference in $^3J_{syn-m}$ and $^3J_{anti-m}$ for the latter (10.2 and 14.5 Hz, respectively) as compared with that in **1** argues for more sp^2-like hybridization for the methylenes of the scandium allyl, contrasting with the more sp^3-like methylenes of the "tantalabicyclobutane" complex, where the two d electrons are engaged in considerable π back-bonding with the allyl ligand:

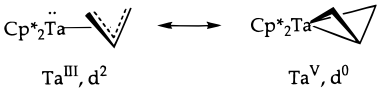

As the temperature of the sample is steadily increased, the ^{1}H NMR spectra for **1** gradually change: at 257 K (500 MHz) the signals for the η^5-C_5Me_5 protons coalesce, at approximately 286 K (500 MHz) the signals for the four methylene protons of the allyl ligand broaden into the baseline, and at higher temperature (326 K, 500 MHz) the five allyl protons give rise to an AX_4 pattern, with average *syn*/*anti* chemical shifts and average $^3J_{H-H}$ values indicative of rapid *syn* ⇄ *anti* interchange. Similar spectral trends are observed for Cp*$_2$Sc(η^3-C_3H_5) in THF-d_8: low-temperature spectra (≤233 K) indicate a static η^3-allyl ligand, coalescence of the Cp* signals is observed at 229 K, and the *syn* and *anti* allyl methylene averaging occurs with a coalescence temperature (T_c) of ∼273 K (300 MHz).

Given the smaller frequency difference for the η^5-C_5Me_5 signals ($\Delta\nu = 65$ Hz at 194 K) *vis à vis* those for the *syn* and *anti* protons ($\Delta\nu = 940$ Hz at 194 K), on gradual warming of the sample one would expect averaging of the η^5-C_5Me_5 signals before averaging those for the *syn* and *anti* protons, if a single fluxional process were occurring. Indeed, the observed exchange of *syn* and *anti* protons of the allyl ligand require that, of the two possible mechanisms shown in Scheme 2, process i, which involves $\eta^3 \rightleftarrows \eta^1$ changes in allyl coordination, must occur. On the other hand, a faster allyl rotation while the group is η^3-coordinated, process 2 in Scheme 2, and a slower process (1) would also result in coalescence of the η^5-C_5Me_5 signals before those for the *syn* and *anti* protons as the temperature is raised.

To distinguish between these alternatives, it was desirable to use line shape fitting routines to calculate the rate constants for exchange at various temperatures. Satisfactory fits to the observed spectra were possible assuming that only process 1 (Scheme 2) is operating with a slow $\eta^3 \rightarrow \eta^1$ step and subsequent fast rotations about the Sc−C and C−C bonds for Cp*$_2$Sc(η^1-C_3H_5) (Scheme 5).

Scheme 5

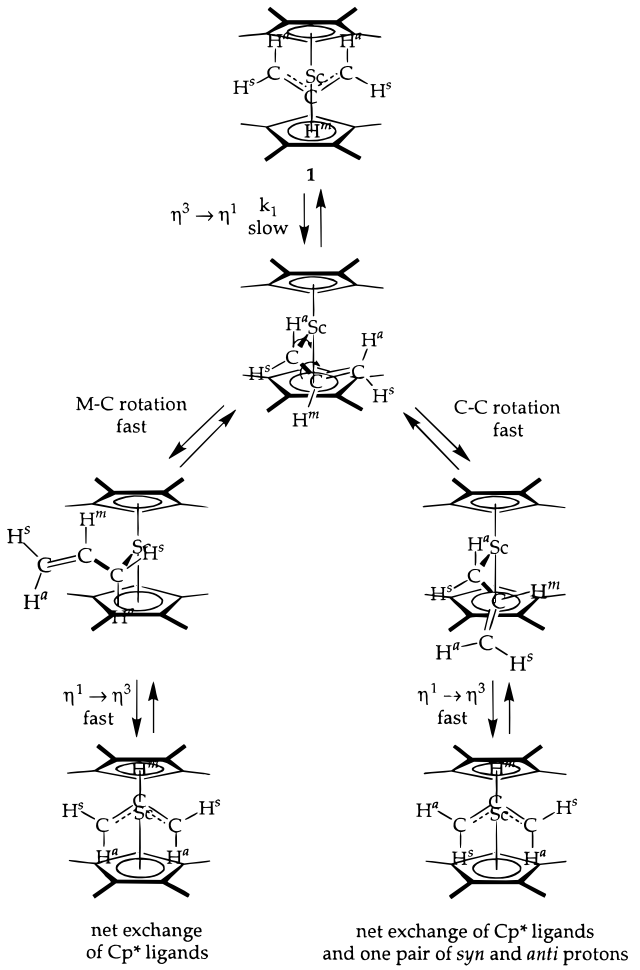

Under these assumptions the rate constant for pentamethylcyclopentadienyl exchange is $^1/_2k_1$, since there is equal likelihood that following the $\eta^3 \rightarrow \eta^1$ step the allyl returns to η^3 coordination with the same or with a 180°-rotated orientation. Moreover, the rate constant for *syn* ⇄ *anti* methylene proton exchange is $^1/_8k_1$, since at least two $\eta^3 \rightarrow \eta^1$ steps (from differing sides of the [Cp*$_2$-Sc] wedge) must occur to effect interchange of both *syn* protons with both *anti* protons, and again there is equal likelihood that, following the $\eta^3 \rightarrow \eta^1$ step, the allyl returns to η^3 coordination with or without interchanging the two α-methylene protons.

Using the rate constants derived from the best fits to the observed spectra near coalescence of Cp* and *syn*

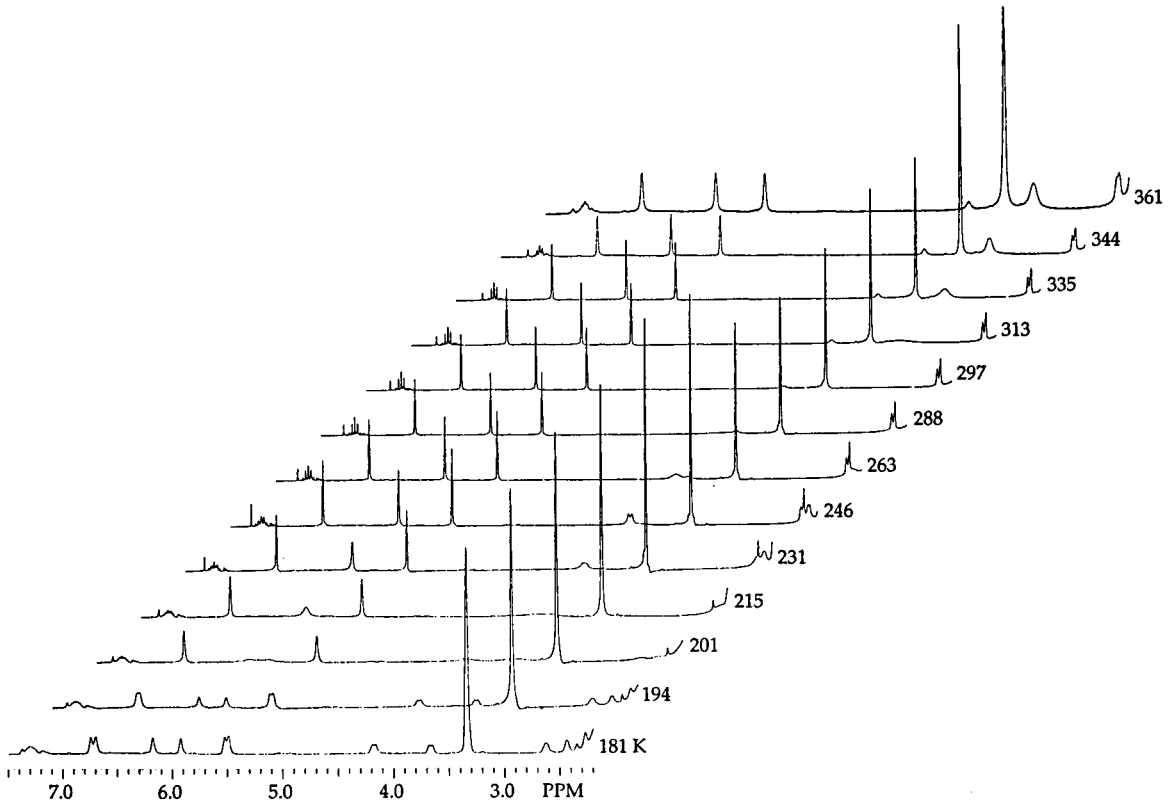

Figure 2. Downfield resonances of the variable-temperature 500 MHz ^{1}H NMR spectra for **4** (Et_2O-d_{10}).

and *anti* methylene protons[17] at two different field strengths (corresponding to 500 and 300 MHz), a fairly linear Eyring plot is obtained, further supporting the assumed fluxionality as arising from a single, rate-determining process. Activation parameters and rate constants for **1** are thus obtained (Table 2): in Et_2O, $\Delta G^{\ddagger} = 11.6 \pm 0.8$ kcal mol^{-1} at 250 K, $\Delta H^{\ddagger} = 8.0 \pm 0.6$ kcal mol^{-1}, and $\Delta S^{\ddagger} = -14 \pm 4$ eu; in THF, $\Delta G^{\ddagger} = 11.6 \pm 0.8$ kcal mol^{-1} at 229 K, $\Delta H^{\ddagger} = 5.5 \pm 0.6$ kcal mol^{-1}, and $\Delta S^{\ddagger} = -23 \pm 4$ eu. The marginally more negative value for the entropy of activation in THF may argue for an associative displacement of the C═C double bond to generate $Cp^*_2Sc(\eta^1\text{-}C_3H_5)$(THF), but the precision of the data is not sufficient to provide confidence in such a conclusion. Our analysis does not unambiguously rule out the occurrence of a slower 180° η^3-C_3H_5 rotation (process 2, Scheme 2), but inclusions of $10k_{rot} < k_1$ do not significantly alter the simulated spectra.

The variable-temperature spectra for the meso allyl complexes are markedly different from those for **1**. At low temperatures the expected AGMPX splitting pattern is exhibited for the allyl ligand, resulting from the inequivalence of the two sides of the metallocene wedges:

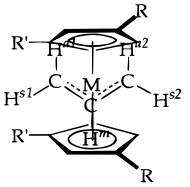

2, M = Sc; R = CMe_3; R' = H
3, M = Sc; R = R' = $CHMe_2$
4, M = Sc; R = 2-2-Me-adamantyl; R' = H
5, M = Y; R = 2-2-Me-adamantyl; R' = H

Shown in Figure 2 are the relevant portions of the variable-temperature ^{1}H NMR spectra for **4** in Et_2O-d_{10}. In addition to the two types of $SiMe_2$ protons (δ 0.25 and 0.75) and the methyladamantyl protons (δ 0.84−2.27), at the lowest temperature (181 K, 500 MHz) the six cyclopentadienyl protons (δ 5.49−6.74) and five allyl protons (δ 7.30 and δ 2.41−4.16) are all inequivalent. As the probe temperature is raised (∼215 K), the resonances for H^{s1} and H^{s2} (δ 2.41 and 2.61) broaden and coalesce, as do the resonances for H^{a1} and H^{a2} (δ 3.64 and 4.16). Continuing to raise the temperature results in the appearance of two new allyl resonances, one located approximately midway between the previous signals for H^{s1} and H^{s2}, and the other resonance midway between those of H^{a1} and H^{a2} (246 K), corresponding to an averaging of the two types of *syn* and two types of *anti* methylene protons of the allyl ligand. Accompanying these changes at higher temperatures are averaging of the protons of the two different cyclopentadienyl ligands and the methyladamantyl substituents. As the temperature of the sample is raised further, the averaged *syn* and averaged *anti* methylene protons (at approximately 2.51 and 3.89 ppm, respectively) in the AM_2X_2 spectra broaden and coalesce, and a new signal grows in, located approximately equidistant from those of the previously averaged H^s and H^a resonances. This AX_4 splitting pattern, where all allyl methylene protons are magnetically equivalent, indicates not only rapid *syn*−*syn* (*anti*−*anti*) exchange, but also rapid exchange of the *syn* and *anti* allyl protons at the highest temperatures.

The same progression from AGMPX to AM_2X_2 to AX_4 splitting patterns for **4** is also observed for **2**, **3**, and **5**, regardless of solvent, although the limiting AX_4 splitting

(17) The fits are most sensitive to the trial rate constants in these temperature regions.

Scheme 6

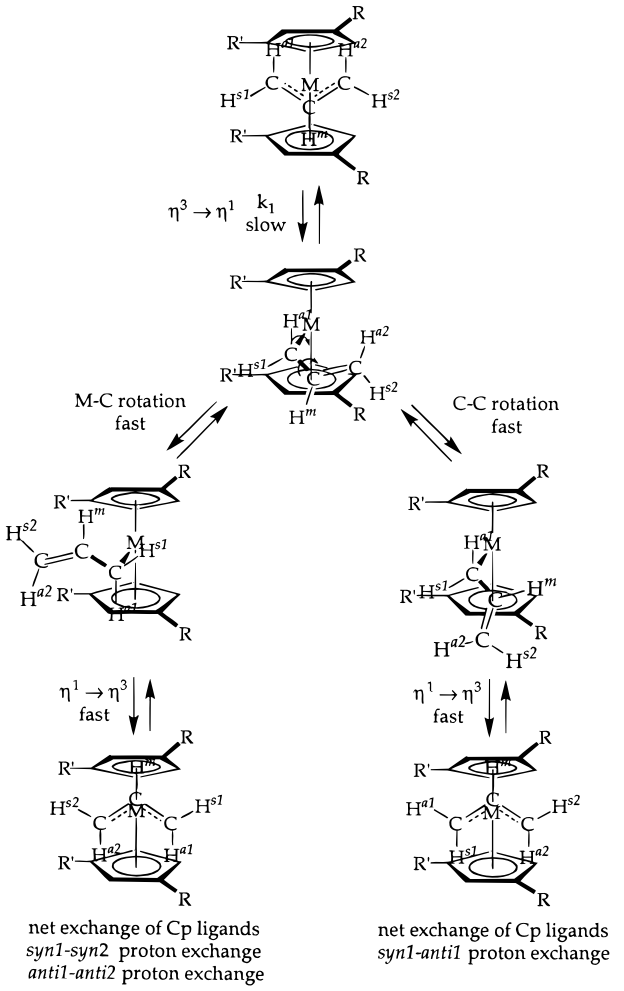

pattern, observed above 358 K at 300 MHz for **2**, is not fully achieved at the highest allowed temperatures for **3** and **5**.

The AX_4 patterns require that for the meso complexes **2**−**5** (as for **1**) $\eta^3 \rightleftarrows \eta^1$ changes in allyl coordination with 180° rotation about the C−C single bonds (process 1, Scheme 2) are fast on the NMR time scale. Thus, at least at the highest temperatures, the processes shown in Scheme 6 are required to obtain the AX_4 spectra.

The AM_2X_2 spectra observed at intermediate temperatures could be argued to arise simply from the smaller chemical shift differences between the two types of *syn* protons, H^{s1} and H^{s2}, and between *anti* protons, H^{a1} and H^{a2}, as compared to the chemical shift differences between *syn* and *anti* protons. Thus, as the temperature is raised, the two signals for the *syn* protons are expected to coalesce and give rise to an average signal (likewise for the signals for the *anti* protons) before those for *syn* protons average with those for the *anti* protons. On the other hand, faster *syn*−*syn* and *anti*−*anti* exchange could arise from faster 180° rotation while the allyl is η^3-coordinated (process 2, Scheme 2) (eq 4).

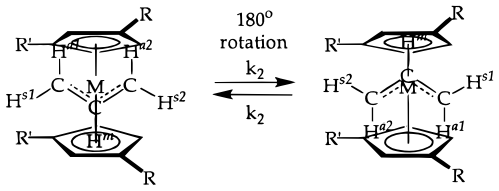

(4)

Thus, the qualitative spectral changes could arise from either possibility A, where process k_2 (eq 4) is slow at all temperatures and process k_1 (Scheme 6) is slow and rate-determining at low temperatures and fast at high temperatures, or possibility B, where processes k_2 and k_1 are slow at the lowest temperatures, process k_2 is fast at intermediate temperatures, and both processes, k_2 and k_1, are fast at the highest temperatures. Distinguishing between these possibilities, in the absence of line shape analysis, proved exceptionally difficult. The temperature range over which the Cp substituents coalesce is extremely narrow; Eyring plots relying on these rate data showed considerable scatter. Moreover, since the two sides of the metallocene wedge are inequivalent for the meso metallocenes, there are in reality two rates of $\eta^3 \rightarrow \eta^1$ conversion for the allyl ligand and a favored side of the metallocene wedge for recoordination of the C=C double bond of the η^1-C_3H_5 intermediate. Thus, the statistical factors relating k_1 to methylene proton exchange rates are not as clear as for more symmetric **1**.[18]

Line shape analysis does strongly suggest possibility B above. Attempts to simulate the variable-temperature spectra for **2**−**5** using only a rate-limiting $\eta^3 \rightarrow \eta^1$ process that succeeded for **1**, failed to successfully model the observed spectra over the entire temperature range investigated. In particular, although the lowest and highest temperature spectra could be modeled, the characteristic AM_2X_2 intermediate spectral pattern could not be obtained solely by varying the rate constant k_1. Similarly, while simulated VT NMR spectra using only the k_2 process do successfully model both the lowest and intermediate temperature spectra, this process cannot, of course, generate the AX_4 pattern observed experimentally at the highest temperatures, since the process in eq 4 does not interchange *syn* and *anti* protons.

The experimentally observed spectra could, however, be successfully simulated using a low barrier η^3 rotation (k_2) process *and* a slower $\eta^3 \rightarrow \eta^1$ (k_1) process. Trial values for k_1 were estimated at several temperatures,[18] including those at coalescence, and the simulations were optimized by varying k_2. Several iterations, using new values for k_1 and reoptimizing with new values for k_2, resulted in internally reasonable values for k_1 and k_2 that simulated the observed spectra over the entire temperature range (see Figure 3 for simulated spectra for **4**).

It should be noted that these simulations semiquantitatively establish that, in order to satisfactorily simulate the intermediate-temperature spectra, both the k_2 and k_1 processes are required to be fast, with $k_2 > k_1$. The simulations do not, however, provide accurate values for k_1 and k_2, so that their values (Table 2) and any activation parameters derived therefrom should be viewed with considerable caution. Moreover, comparisons among the allyl complexes of meso metallocenes **2**−**5** are difficult to make, since $\Delta G^{\ddagger}$ values, while apparently not particularly temperature-dependent (implying $\Delta S^{\ddagger}$ values are close to zero), are strictly comparable only at a common temperature. Nonetheless,

(18) If the k_2 process is fast, a k_1 process that preferentially occurs from one side of the metallocene wedge will exchange both *syn* protons with both *anti* protons, and the rate constant for *syn* ⇄ *anti* exchange will be $^1/_4 k_1$.

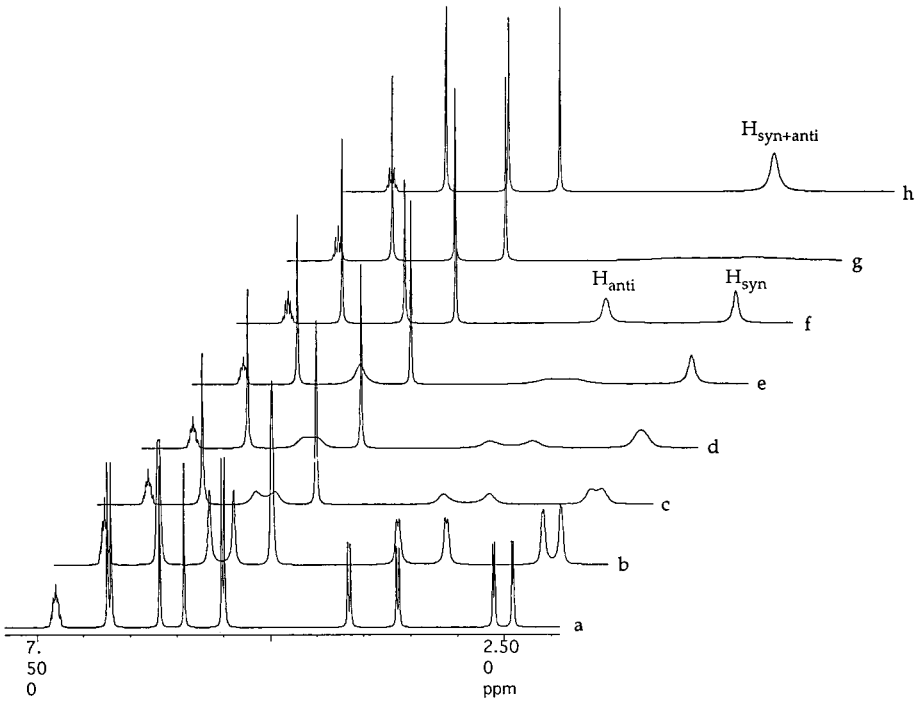

Figure 3. gNMR simulations of 500 MHz ^{1}H NMR spectra for allylic and cyclopentadienyl resonances for **4**: (a) low-temperature limit ($k_1 = k_2 = 0$); (b) 197 K ($k_1 = 2$ s^{-1}, $k_2 = 35$ s^{-1}); (c) 201 K ($k_1 = 3$ s^{-1}, $k_2 = 170$ s^{-1}); (d) 207 K ($k_1 = 6$ s^{-1}, $k_2 = 260$ s^{-1}); (e) 215 K ($k_1 = 15$ s^{-1}, $k_2 = 550$ s^{-1}); (f) 246 K ($k_1 = 260$ s^{-1}, $k_2 = 2.0 \times 10^4$ s^{-1}); (g) 290 K ($k_1 = 5.2 \times 10^3$ s^{-1}, $k_2 = 7.1 \times 10^5$ s^{-1}); (h) 344 K ($k_1 = 7.4 \times 10^4$ s^{-1}, $k_2 = 1.7 \times 10^7$ s^{-1}).

some conclusions can be reached on the basis of these semiquantitative rates and activation barriers for $\eta^3 \rightarrow \eta^1$ conversion and η^3 rotation: (1) both η^3-rotation and $\eta^3 \rightarrow \eta^1$ conversion occur at rates comparable to the NMR time scale (at accessible temperatures), (2) for all four complexes η^3 rotation is considerably faster with barriers approximately 1.2−4.9 kcal mol^{-1} lower than those for $\eta^3 \rightarrow \eta^1$ conversion, and (3) the $\eta^3 \rightarrow \eta^1$ process is considerably slower for the yttrium complex **5**, as compared with the three scandocene allyls, yet the barrier for η^3 rotation is intermediate. The qualitative ordering of decreasing rates among the scandocene allyl complexes for the $\eta^3 \rightarrow \eta^1$ process (**4** > **2** > **3**) may be attributed to steric destabilization of the η^3-C_3H_5 coordination mode, with steric congestion expected to decrease in the order R = 2-2-Me-adamantyl > R = CMe_3 > R = $CHMe_2$. The reasons for the qualitative ordering of decreasing rates for η^3 rotation (**4** ≈ **5** > **3** ≈ **2**) is less obvious, although the difference in activation barriers among the series amounts to only approximately 2 kcal mol^{-1}.

Variable-temperature NMR spectra for the third class of allyl complexes, those for which the allyl ligand is bonded to racemic scandocenes, complexes **6** and **7**, are again distinct. The C_2-symmetric ligand array results in pronounced differences from the C_{2v} ligand of **1** and C_s-symmetric ligands of **2**−**5**. Thus, at low temperatures AGMPX allyl splitting patterns and inequivalent cyclopentadienyl resonances are observed for **6** and **7**, attributable to static η^3-C_3H_5 structures:

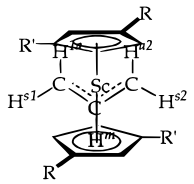

As the probe temperature is raised, the cyclopentadienyl substituents become equivalent, and at higher temperatures there is simultaneous broadening of all four signals for the allyl methylene protons. These signals remain broadened into the baseline over a broad temperature range, until at the highest temperatures a single resonance appears at approximately the weighted average of the signals for the four methylene protons. Thus, the AGMPX pattern is replaced by an AX_4 one, with no intermediate AM_2X_2 pattern, as is observed for **2**−**5**.

These observations are compatible with both (faster) η^3 rotation and $\eta^3 \rightarrow \eta^1$ processes, as for the allyl complexes of the closely related meso metallocenes, although the consequences of the two steps are somewhat different for the racemic metallocene complexes. As shown in eq 5, η^3 rotation interchanges cyclopentadienyl ligands but, unlike the case for **2**−**5**, does *not* interchange the two types of *syn* and two types of *anti* methylene protons. Generation of AX_4 patterns for **6** and

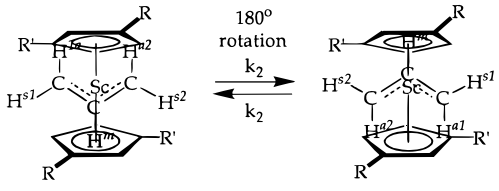

(5)

7 again requires interchange of *syn* and *anti* methylene protons, again most likely via rate-determining $\eta^3 \rightarrow \eta^1$ conversion (Scheme 7). Rotation about the Sc−C bond of the η^1-C_3H_5 intermediate results in the same net effect as η^3 rotation, while rotation about the C−C bond of the η^1-C_3H_5 intermediate leads to simultaneous interconversion of one pair of *syn* and *anti* methylene

Scheme 7

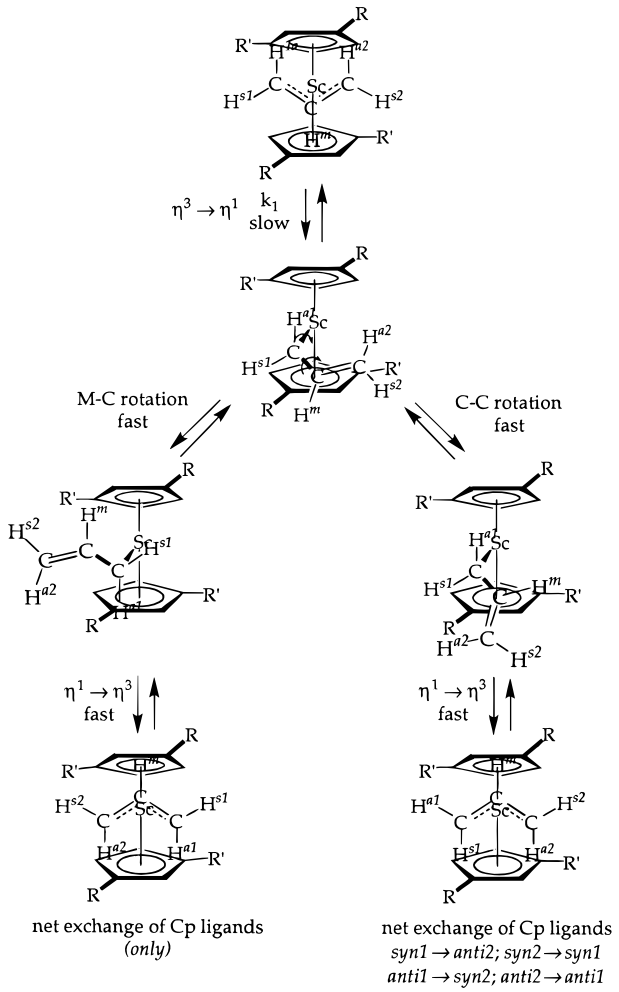

protons with interconversion of the complementary pair of *syn* with *syn* and *anti* with *anti* methylene protons.

Spectral simulations near coalescence, although not particularly precise since the allyl methylene protons are broadened into the baseline over such a broad range of intermediate temperatures, provide estimates of k_1 and $\Delta G^{\ddagger}$: for **6**, $k_1(359\ \text{K}) = 8.4 \times 10^3\ \text{s}^{-1}$, $\Delta G^{\ddagger} = 14.7 \pm 1.0$ kcal mol^{-1} in toluene-d_8 and $k_1(359\ \text{K}) = 5.2 \times 10^3\ \text{s}^{-1}$, $\Delta G^{\ddagger} = 14.6 \pm 1.0$ kcal mol^{-1} in THF-d_8; for **7**, $k_1(330\ \text{K}) = 6.4 \times 10^3\ \text{s}^{-1}$, $\Delta G^{\ddagger} = 13.6 \pm 1.0$ kcal mol^{-1} in toluene-d_8 and $k_1(335\ \text{K}) = 6.8 \times 10^3\ \text{s}^{-1}$, $\Delta G^{\ddagger} = 13.8 \pm 1.0$ kcal mol^{-1} in THF-d_8.[19] The values for racemic **6** are comparable to those for the corresponding meso isomer **3** (Table 2). Likewise, the rates and barriers for enantiopure **7**, having two *tert*-butyl substituents in β-positions relative to the linking silicon atom, compare to those for the corresponding meso isomer **2**. These similarities could be taken to suggest that rate of the $\eta^3 \rightarrow \eta^1$ process depends more on the size of the cyclopentadienyl substituents than their placement in the wedge.

Conclusions

Variable-temperature ^{1}H NMR experiments on the allyl complexes **1**−**7** indicate in all cases a static η^3-C_3H_5 solution structure, analogous to that established by X-ray diffraction for *rac*-$Me_2Si[\eta^5$-2,4-$(CHMe_2)_2$-$C_5H_2]_2$-$Sc(\eta^3$-$C_3H_5)$. At the highest temperatures *syn* ⇄ *anti* interchange is fast on the ^{1}H NMR time scale for all seven complexes, implicating a $\eta^3 \rightleftarrows \eta^1$ process. Line shape analysis provides estimates of the rate constants and activation free energies for the $\eta^3 \rightarrow \eta^1$ step. The symmetry of the allyl derivatives of the meso *ansa*-scandocenes or -yttrocene, **2**−**5**, distinguishes the two types of *syn* and *anti* protons, and the observation of faster *syn*−*syn* and *anti*−*anti* exchange further implicates another process, η^3 rotation. For **2**−**5** satisfactory fits to the observed ^{1}H NMR spectra indicate that the η^3 rotation process is 1−2 orders of magnitude faster that the $\eta^3 \rightarrow \eta^1$ process. On the other hand, for more sterically crowded **1**, η^3 rotation appears to be slower than the $\eta^3 \rightarrow \eta^1$ process. Unfortunately, the precision of the rate constants that can be extracted from the spectral fits does not allow determination of activation enthalpies and activation entropies. Thus, strict comparisons of the rates and barriers at a common temperature cannot be made. On the other hand, it is likely that activation entropies for the intramolecular $\eta^3 \rightarrow \eta^1$ process are small, so that the temperature dependence of the activation free energies likely is also small. Under this assumption, the rates follow the order **4** > **2** > **3**, the decreasing order of size for the β-substituents of the *ansa*-scandocenes. Slower $\eta^3 \rightarrow \eta^1$ for the yttrium analogue of **4** with approximately 4 kcal mol^{-1} higher activation free energy is in accord with both the higher metal−olefin bond dissociation energy expected for the heavier congener and less steric crowding for the η^3-C_3H_5 ground state for larger yttrium. It is remarkable that $\Delta G_1^{\ddagger}$ values for the seven complexes fall in the relatively narrow range 11−16 kcal mol^{-1} (11−15 kcal mol^{-1} for the six scandocene derivatives). These values represent upper limits on the strength of the metal−olefin interaction for this special class of chelated olefin adducts. The barriers for zirconium−olefin and yttrium−olefin dissociation determined by Jordan[7] ($\Delta G^{\ddagger}$ = 10.7 kcal mol^{-1}), Casey[8] ($\Delta G^{\ddagger}$ < 10.4 kcal mol^{-1})[8b] and Royo[9] ($\Delta G^{\ddagger}$ = 11.4 kcal mol^{-1}) fall slightly below this range, the difference possibly reflecting the loss in resonance stabilization for the η^3-allyl compounds on dissociation of the C=C double bond. That some seemingly closely related complexes, *e.g.* $(\eta^5$-$C_5Me_5)_2Nd(\eta^3$-$C_3H_5)$,[5b] have barriers for the $\eta^3 \rightarrow \eta^1$ process that must exceed ca. 20 kcal mol^{-1} is remarkable but must reflect much reduced steric crowding for the much larger lanthanide derivatives.

Experimental Section

General Considerations. All air- and/or moisture-sensitive compounds were manipulated using standard high-vacuum-line, Schlenk, or cannula techniques or in a glovebox under a nitrogen atmosphere, as described previously.[20] Argon and hydrogen gases were purified and dried by passage through columns of MnO on vermiculite and activated 4 Å molecular sieves. Solvents were stored under vacuum over a form of "titanocene"[21] or sodium benzophenone ketyl. The

(19) Since the two sides of the metallocene wedge are the same for the racemic isomers, the statistical factor here is the same as for the more symmetric **1**.

(20) Burger, B. J.; Bercaw, J. E. *New Developments in the Synthesis, Manipulation, and Characterization of Organometallic Compounds*; Wayda, A., Darensbourg, M. Y., Eds.; American Chemical Society: Washington, DC, 1987; Vol. 357.

(21) Marvich, R. H.; Brintzinger, H. H. *J. Am. Chem. Soc.* **1971**, *93*, 2046.

preparations of *meso*-[{$Me_2Si(C_5H_3$-3-$CMe_3)_2$}$_2$ScH]$_2$,[22] Cp*$_2$ScH,[4a] and *meso*- (**3**) and *rac*-{$Me_2Si[C_5H_2$-2,4-$(CHMe_2)_2]_2$}Sc(η^3-C_3H_5)[15] (**6**) were carried out as previously reported. Potassium hexamethyldisilazide was purchased (Aldrich) and sublimed prior to use (10^{-4} mmHg/160 °C). Pyrrolidine, 2-adamantanone, methyllithium, butyllithium, allylmagnesium bromide, allene, and dicyclopentadiene were purchased (Aldrich) and used as received.

NMR spectra were recorded on General Electric QE300 (300 MHz for ^{1}H) and Bruker AM500 (500.13 MHz for ^{1}H) spectrometers. Elemental analyses were carried out at the Caltech Elemental Analysis Facility by Fenton Harvey. Many of the compounds failed to give satisfactory carbon/hydrogen analyses, even when combusted with added V_2O_5 oxidant. Moreover, in many cases the results were inconsistent from run to run.

Preparation of *meso*-$Me_2Si(\eta^5$-3-CMe_3-$C_5H_3)_2Sc(\eta^3$-$C_3H_5)$ (2). In an inert-atmosphere glovebox, a J-Young NMR tube was charged with approximately 15 mg (0.0218 mmol) of *meso*-[{$Me_2Si(C_5H_3$-3-$CMe_3)_2$}ScH]$_2$ and 0.4 mL of benzene-d_6. After the solution was degassed at −78 °C, allene (0.111 mmol) was measured into the NMR tube using a calibrated gas bulb. The solution was then heated at 80 °C for 6 h, at which time the volatiles were removed from the NMR tube *in vacuo*. The resulting yellow solid was dried under dynamic vacuum for an additional 30 min. ^{1}H NMR (25 °C, benzene-d_6): δ 7.50 (m, CH_2CHCH_2, 1H), 6.75 (t, C_5H_3, 2H, J = 2.5 Hz), 5.96 (s (br), C_5H_3, 2H), 5.29 (t, C_5H_3, 2H, J = 2.6 Hz), 4.33 (s (br), *anti*-CH_2CHCH_2, 2H), 2.25 (s (br), *syn*-CH_2CHCH_2, 2H), 1.08 (s, CMe_3, 18H), 0.70 (s, $SiMe_2$, 3H), 0.22 (s, $SiMe_2$, 3H).

Preparation of 6,6′-(Tricyclo[3.3.1.1]decane)fulvene. To a stirred solution of 2-adamantanone (24.85 g, 165.4 mmol) and freshly cracked cyclopentadiene (66.0 mL, 800.6 mmol) in 500 mL of methanol was added 17.0 mL (204 mmol) of pyrrolidine. Yellow solid began precipitating from the burgundy colored solution within several hours. After it was stirred for 11 days, the solution was acidified with 33 mL of glacial acetic acid and diluted with 400 mL of water and 100 mL of diethyl ether. The liquids were transferred to a 2 L separatory funnel, to which was added an additional 100 mL of water and 400 mL of ether. The aqueous layer was washed three times with 375 mL and once with 75 mL of ether, and the combined organic layers were washed once with 150 mL of water and once with 150 mL of brine. After it was dried over and gravity filtered from magnesium sulfate, the organic solution was reduced to dryness with a rotary evaporator, leaving an orange-brown solid. Bright yellow crystals (28.69 g, 144.7 mmol, 88% yield) were obtained upon recrystallization from petroleum ether. Anal. Calcd for $C_{15}H_{18}$: C, 90.83; H, 9.17. Found (with V_2O_5 added): C, 90.97, 90.92; H, 8.97, 9.05. ^{1}H NMR (benzene-d_6): δ 6.65 (m, C_5H_4, 2H) and 6.62 (m, C_5H_4, 2H), 3.11 (s, $C_{10}H_{14}$, 2H), 1.75 (t, $C_{10}H_{14}$, 8H, J = 2.59 Hz), 1.72 (q, $C_{10}H_{14}$, 2H, J = 2 Hz), 1.65 (t, $C_{10}H_{14}$, 2H, J = 2.75 Hz).

Preparation of [2-(2-CH_3)-$C_{10}H_{14}$]C_5H_4Li·TMEDA. A 2 L three-necked round-bottom flask, equipped with a rubber septum, a 180° needle valve adapter, and a magnetic stir bar was charged with 83.30 g (420 mmol) of 6,6′-(tricyclo[3.3.1.1]-decane)fulvene. With stirring, 1100 mL of diethyl ether and 64 mL (424 mmol, 1.01 equiv) of *N*,*N*,*N*′,*N*′-tetramethylethylenediamine were added to the flask via cannula. The solution was cooled to 0 °C, and a 1.4 M methyllithium solution (Et_2O, 300 mL, 420 mmol) was added to the flask via cannula over 1 h. White solid began to precipitate from the otherwise clear and bright yellow solution during the methyllithium addition. The solution was warmed slowly to 25 °C and was stirred for 6 days. The solvent was removed *in vacuo*, and the remaining white solid was washed four times with 150 mL aliquots of petroleum ether followed by filtration. The petroleum ether insoluble material was dried *in vacuo* for 6 h, providing 132.5 g (393.7 mmol, 94% yield) of a fluffy white solid. Anal. Calcd for $C_{22}H_{37}N_2Li$: C, 78.51; H, 11.10; N, 8.33. Found (with V_2O_5 added): C, 77.95, 78.43; H, 10.30, 11.03; N, 8.29, 8.46. ^{1}H NMR (THF-d_8): δ 5.57 (m, C_5H_4, 2H), 5.56 (m, C_5H_4, 2H), 2.39 (d, $C_{10}H_{14}$, 2H, J = 5.66 Hz), 2.26 (s, TMEDA, 4H), 2.22 (s, $C_{10}H_{14}$, overlaps with TMEDA), 2.13 (s, TMEDA, 14 H), 2.07 (s, $C_{10}H_{14}$, 2H), 1.83 (s, $C_{10}H_{14}$, 1H), 1.69, 1.65 (s, $C_{10}H_{14}$, overlapping, 4H total), 1.59 (s, $C_{10}H_{14}$, 1H), 1.42 (d, $C_{10}H_{14}$, 2H, J = 5.91 Hz), 1.30 (s, 2-CH_3, 3H).

Preparation of Me_2Si{3-[2-(2-CH_3)-$C_{10}H_{14}$]-C_5H_4}$_2$. A 2 L three-necked round-bottom flask, equipped with a 180° needle valve adapter and a rubber septum, was charged with 80.82 g (237.7 mmol) of [2-(2-CH_3)-$C_{10}H_{14}$]C_5H_4Li·TMEDA. THF (400 mL) was added via cannula, and the contents of the flask were cooled to −78 °C. Dichlorodimethylsilane (13.5 mL, 111.1 mmol) was vacuum-transferred from CaH_2 into an evacuated 50 mL round-bottom flask/180° needle valve assembly. The Me_2SiCl_2 was then syringed slowly into the 2 L flask containing the white THF suspension. The THF solution was slowly warmed to room temperature and stirred for an additional 36 h. THF was removed *in vacuo*, leaving a viscous yellow oil which was brought into an inert-atmosphere glovebox. The petroleum ether insoluble white solid was removed by suction filtration inside the glovebox, and the bright yellow filtrate was transferred to a 1 L round-bottom flask with a 180° needle valve adapter. Solvent was removed *in vacuo*, leaving a large quantity of viscous orange oil. [2-(2-CH_3)-$C_{10}H_{14}$]C_5H_5, a side product from the linking reaction, was removed by Kugelröhr distillation (15 h, 100 °C, $<1 \times 10^{-3}$ Torr), affording 42.7 g (88 mmol, 79% yield) of Me_2Si{3-[2-(2-CH_3)-$C_{10}H_{14}$]-C_5H_4}$_2$ as a dark orange-brown glassy solid upon cooling to room temperature. Anal. Calcd for $C_{34}H_{48}Si$: C, 84.21; H, 10.00. Found (with V_2O_5 added): C, 83.15, 82.97; H, 10.30, 9.75. Found (without added V_2O_5): C, 83.22, 83.12; H, 8.73, 8.58. ^{1}H NMR (benzene-d_6): δ 6.66, 6.53, 6.18 (C_5H_4, 6H total), 3.31, 3.04, 3.01 (C_5H_4, 2H total), 2.27, 2.26, 2.20, 2.16, 2.14, 2.11, 2.06, 1.85, 1.78, 1.71, 1.65, 1.63, 1.60, 1.58 ($C_{10}H_{14}$, 43H total), 1.25, 1.24, 1.22, 1.20, 1.13 (2-CH_3, 6H), 0.17, 0.14, −0.13, −0.14, −0.18 ($SiMe_2$, 5H total).

Author: What do you mean by "<1 μ" above?

Preparation of Me_2Si{3-[2-(2-CH_3)-$C_{10}H_{14}$]-C_5H_3}$_2$Li$_2$. A 500 mL round-bottom flask equipped with a magnetic stir bar and a 180° needle valve adapter was charged in a drybox with 8.7 g (18.0 mmol) of Me_2Si{3-[2-(2-CH_3)-$C_{10}H_{14}$]-C_5H_4}$_2$. Petroleum ether (160 mL) was vacuum-transferred onto the orange solid, and the solution was cooled to 0 °C. A 1.6 M solution of *n*-butyllithium in hexanes (24 mL, 38.4 mmol) was syringed into the round-bottom flask against an argon counterflow over a period of 5 min. The solution was warmed slowly to room temperature and stirred for 16 h. The volatiles were removed under reduced pressure from the suspension, and the resulting beige solid was dried *in vacuo* for an additional 2 h. In an inert-atmosphere glovebox the flask was attached to a fine-porosity swivel frit and a 500 mL round-bottom flask. Petroleum ether (175 mL) was added to the solid by vacuum transfer, and the solution was filtered after being warmed to room temperature. Solvent was removed, and the beige petroleum ether insoluble material was dried *in vacuo* for 8 h, affording 8.20 g of a pale peach colored solid. The product was recrystallized from Et_2O, yielding 4.76 g (9.58 mmol, 53.2% yield) of ligand; additional material may probably be recovered from the remaining 1.95 g of Et_2O-soluble material through additional recrystallizations. Anal. Calcd for $C_{34}H_{46}SiLi_2$: C, 82.20; H, 9.35. Found (with V_2O_5 added): C, 79.91, 78.31; H, 10.05, 9.54. ^{1}H NMR (THF-d_8): δ 5.91 (t, C_5H_3, 2H, J = 2.54 Hz), 5.90 (t, C_5H_3, 2H, J = 2.05 Hz), 5.70 (t, C_5H_3, 2H, J = 2.58 Hz), 2.41 (d, J = 4.89 Hz), 2.24 (d, J = 5.63 Hz), 2.10, 1.83, 1.69, 1.66 (d, J = 6.41 Hz), 1.58, 1.41(d, J = 5.92 Hz) ($C_{10}H_{14}$, 28 H total), 1.27 (s, 2-CH_3, 6H), 0.24 (s, $SiMe_2$, 6H).

(22) Bunel, E.; Burger, B. J.; Bercaw, J. E. *J. Am. Chem. Soc.* **1988**, *110*, 976.

Preparation of *meso*-$Me_2Si\{\eta^5$-3-[2-(2-CH_3)-$C_{10}H_{14}$]-$C_5H_3\}_2ScCl-LiCl\cdot 2THF$. In a 100 mL round-bottom flask attached to a medium-porosity swivel frit was placed a magnetic stir bar, 2.09 g (4.21 mmol) of $Me_2Si\{3$-[2-(2-CH_3)-$C_{10}H_{14}$]-$C_5H_3\}_2Li_2$, and 1.54 g (4.19 mmol) of $ScCl_3(THF)_3$. THF (50 mL) was added to the flask by vacuum transfer, and the resulting solution was warmed to room temperature. After 45 min of stirring, all the reagents had fully dissolved, producing a clear, orange solution. The THF was removed under reduced pressure after the mixture was stirred for 12 h, and the resulting tan foam was dried *in vacuo*. In a glovebox, the foam was crushed into a finely divided solid, and the flask was reattached to the frit assembly. Petroleum ether (50 mL) was transferred onto the solid, and the solution was warmed to 25 °C. The tan petroleum ether insoluble species was removed by filtration and washed three times with small portions of petroleum ether. Removal of solvent from the petroleum ether solution provided 0.374 g (0.50 mmol) of product. Additional product comprised much of the 1.86 g of petroleum ether insoluble solid (as evidenced by ^{1}H NMR). Anal. Calcd for $C_{42}H_{62}Cl_2LiO_2ScSi$: C, 67.28; H, 8.33. Found: C, 59.06, 59.06, 58.95; H, 7.66, 7.55, 7.52. ^{1}H NMR (THF-d_8): δ 6.23 (t, C_5H_3, 2H, J = 2.5 Hz), 5.89 (t, C_5H_3, 2H, J = 2.1 Hz), 5.79 (t, C_5H_3, 2H, J = 2.7 Hz), 2.50, 2.32, 2.29, 2.25, 2.22, 1.72, 1.69, 1.63, 1.53, 1.49, 1.42, 1.47 (not fully resolved, $C_{10}H_{14}$, 25H total), 2.16 (s, 2-CH_3, 6H), 0.55 (s, $SiMe_2$, 3H), 0.41 (s, $SiMe_2$, 3H).

Preparation of *meso*-$Me_2Si\{\eta^5$-3-[2-(2-CH_3)-$C_{10}H_{14}$]-$C_5H_3\}_2YCl\cdot LiCl(solv)_2$. A 500 mL round-bottom flask, equipped with a magnetic stir bar and 180° needle valve adapter, was charged with 11.15 g of $Me_2Si\{3$-[2-(2-CH_3)-$C_{10}H_{14}$]-$C_5H_3\}_2Li_2$ (22.44 mmol) and 9.23 g of $YCl_3(THF)_{3.5}$ (22.43 mmol). THF (250 mL) was added to the solids by vacuum transfer at −78 °C. The solution was stirred and warmed to room temperature. After 4 days, 150 mL of solvent was removed *in vacuo*, and the solution was stirred for an additional 12 h. The remaining THF was then removed *in vacuo*, affording 19.65 g of tan solid. A portion of the solid (13.73 g) was placed in a 500 mL round-bottom flask, which was attached to a fine-porosity frit and another 500 mL flask. Diethyl ether (150 mL) was added to the solid by vacuum transfer, the solution was warmed to room temperature, and the solvent was then removed *in vacuo*. This procedure was repeated with one 150 mL portion of toluene, and then with two portions of Et_2O. Another 150 mL of diethyl ether was then added by vacuum transfer, and the Et_2O-insoluble material was removed by filtration and washed twice with small portions of ether. Solvent was removed from the dark yellow solution, and the resulting tan foam was washed with an additional 75 mL of Et_2O, which was then removed *in vacuo*. After the resulting foam was dried *in vacuo* for 5 h, 7.19 g of a tan solid was isolated. NMR spectroscopy indicates the presence of 0.16 equiv of toluene, 0.37 equiv of THF, and 1.74 equiv of Et_2O, providing a yield of 8.76 mmol of *meso*-$[Me_2Si\{3$-[2-(2-CH_3)-$C_{10}H_{14}$]-$C_5H_3\}_2]YCl\cdot LiCl$ (56%, based on Y). Anal. Calcd for $C_{42}H_{66}Cl_2LiO_2SiY$ (calcd for a $2Et_2O$ adduct): C, 63.23; H, 8.34. Found: C, 68.61, 68.61; H, 7.09, 7.72. ^{1}H NMR (THF-d_8): δ 6.20 (t, C_5H_3, 2H, J = 2.5 Hz), 5.92 (t, C_5H_3, 2H, J = 2.0 Hz), 5.84 (t, C_5H_3, 2H, J = 2.7 Hz), 2.49, 2.29, 2.24, 2.22, 2.15, 1.82, 1.59, 1.55, 1.43, 1.28 (not fully resolved, $C_{10}H_{14}$, 28H total), 1.69 (s, 2-CH_3, 6H), 0.57 (s, $SiMe_2$, 3H), 0.44 (s, $SiMe_2$, 3H).

Preparation of *meso*-$Me_2Si\{\eta^5$-3-[2-(2-CH_3)-$C_{10}H_{14}$]-$C_5H_3\}_2Sc(\eta^3$-C_3H_5) (4). In an inert-atmosphere glovebox in a 100 mL round-bottom flask was placed 1.87 g (2.5 mmol) of *meso*-$[Me_2Si\{3$-[2-(2-CH_3)-$C_{10}H_{14}$]-$C_5H_3\}_2]ScCl\cdot LiCl\cdot 2THF$ and a magnetic stir bar. The flask was attached to a 180° needle valve adapter, and Et_2O (~50 mL) was added by vacuum transfer. The resulting maroon solution was warmed to room temperature and then cooled back to −78 °C. A 1.0 M solution of allylmagnesium bromide (2.5 mL, 2.5 mmol) was injected against a strong argon counterflow. The solution was stirred at −78 °C for 15 min, after which time the cooling bath was removed, and the solution was warmed to room temperature. After the mixture was stirred at 25 °C for 6 h, the solvent was removed and the resulting brown foam was dried *in vacuo* for 10 h. The flask was then attached to a medium-porosity pencil frit equipped with a 100 mL round-bottom flask and a 90° needle valve adapter. Two 20 mL aliquots of petroleum ether were successively vacuum-transferred onto and off of the brown solid, followed by a similar procedure using 20 mL of toluene and two additional petroleum ether washes (40 mL each) to remove residual THF from the LiCl and Mg halide byproducts prior to filtration. The final petroleum ether solution was filtered, and the solvent was removed *in vacuo*, leaving a dark yellow powder. This powder was dried *in vacuo* for approximately 6 h, affording 480 mg (0.84 mmol, 34% yield) of product. Contamination of the starting material with excess LiCl does not affect the purity or yield of the η^3-C_3H_5 product, as the crude reaction mixture from $Me_2Si\{3$-[2-(2-CH_3)-$C_{10}H_{14}$]-$C_5H_3\}_2Li_2$ and $ScCl_3(THF)_3$ can also be alkylated cleanly with C_3H_5MgBr. Anal. Calcd for $C_{37}H_{51}SiSc$: C, 78.11; H, 9.05. Found (with V_2O_5 added): C, 78.85, 75.78; H, 10.50, 9.98. Found (without V_2O_5): C, 74.90, 75.50; H, 9.13, 9.57. ^{1}H NMR (25 °C, benzene-d_6): δ 7.19 (m, CH_2CHCH_2, overlaps with residual protons of benzene-d_6), 6.55 (t, C_5H_3, 2H, J = 2.47 Hz), 5.98 (t, C_5H_3, 2H, J = 2.40 Hz), 5.54 (t, C_5H_3, 2H, J = 2.57 Hz), 2.39 (d), 2.08 (s), 2.06 (s), 1.92 (d), 1.78 (s), 1.70 (s), 1.67 (s), 1.66 (s), 1.62 (s), 1.59 (s), 1.57 (s), 1.55 (s), 1.49 (s), 1.46 (s) ($C_{10}H_{14}$, 29 H total), 0.85 (s, 2-CH_3, 3H), 0.69 (s, $SiMe_2$, 3H), 0.23 (s, $SiMe_2$, 3H). The *syn* and *anti* resonances on the allyl ligand cannot be located at this temperature.

Preparation of *meso*-$Me_2Si\{\eta^5$-3-[2-(2-CH_3)-$C_{10}H_{14}$]-$C_5H_3\}_2Y(\eta^3$-C_3H_5) (5). In an inert-atmosphere glovebox, a 250 mL round-bottom flask was charged with a magnetic stir bar and 3.24 mmol of *meso*-$[Me_2Si\{3$-[2-(2-CH_3)-$C_{10}H_{14}$]-$C_5H_3\}_2]$-$YCl\cdot LiCl\cdot 2solv$. The flask was then attached to a medium-sized coarse frit with another 250 mL round-bottom flask. Diethyl ether (120 mL) was added by vacuum transfer, and the solution was warmed slightly with stirring, giving a clear tan solution. Against a strong counterflow of argon a solution of allylmagnesium bromide in Et_2O (3.5 mL, 3.5 mmol) was syringed into the solution at −78 °C. After 10 min of stirring at −78 °C the cooling bath was removed, and the solution was warmed to room temperature. After 3 h, 60 mL of Et_2O was removed *in vacuo*, and the solution was stirred for another 5 h. The mixture was then filtered, and the fine white insoluble material was washed once with a small portion of Et_2O. The solvent was removed, leaving a large amount of orange foam which was dried *in vacuo* overnight. The flask containing the Et_2O-soluble species was then attached to a fine pencil frit, and 40 mL of benzene was added by vacuum transfer. The solution was warmed to room temperature and filtered. The benzene was removed *in vacuo*, and the benzene-soluble species was dried for 6 h, leaving 1.70 g of a yellow microcrystalline solid (2.77 mmol, 85% yield). Anal. Calcd for $C_{37}H_{51}SiY$: C, 72.52; H, 8.39. Found: C, 70.37, 70.12, 70.14; H, 8.73, 8.63, 8.72. ^{1}H NMR (25 °C, benzene-d_6): δ 6.72 (m, CH_2CHCH_2, 1H), 6.12 (d, C_5H_3, 2H, J = 2.5 Hz), 5.98 (d, C_5H_3, 2H, J = 2.5 Hz), 5.79 (t, C_5H_3, 2H, J = 2.5 Hz), 3.39 (d, *anti*-CH_2CHCH_2, 2H, J = 7.41 Hz), 2.66, (s (br), *syn*-CH_2CHCH_2, 2H), 2.04 (s), 2.00 (s), 1.98 (s), 1.94 (s), 1.86 (s), 1.78 (s), 1.65 (s), 1.60 (m), 1.58 (s), 1.56 (m), 1.54 (m), 1.51 (m), 1.48 (m), 1.45 (m) ($C_{10}H_{14}$, 29 H total), 0.97 (s, 2-CH_3, 6H), 0.72 (s, $SiMe_2$, 3H), 0.41 (s, $SiMe_2$, 3H).

Preparation of (*R,S*)-$(C_{20}H_{12}O_2)Si(\eta^5$-2-$SiMe_3$-4-$CMe_3C_5H_2)_2ScCl$. The (*R*)-$[(C_{20}H_{12}O_2)Si(C_5H_2$-2-$SiMe_3$-4-$CMe_3)_2]K_2$ ligand used in the following protocol was prepared by a modification of the literature procedure[13c] for the preparation of (*R*)BnBpK$_2$. In an inert-atmosphere glovebox, a 500 mL Schlenk flask was loaded with (*R*)-$[(C_{20}H_{12}O_2)Si(C_5H_3$-2-$SiMe_3$-4-$CMe_3)_2]$ (10.00 g, 14.26 mmol) and $KN(SiMe_3)_2$ (5.83 g, 29.22 mmol). Freshly distilled diethyl ether (250 mL) was added to the solids by vacuum transfer at −78 °C, and the resulting

solution was stirred at this temperature until the ligand had fully precipitated from solution. The white suspension was warmed to room temperature and was stirred for an additional 3 h. Approximately 200 mL of petroleum ether was added, and the suspension was filtered. The white solid was washed with petroleum ether and dried under vacuum (9.1 g, 82% yield).

In an inert-atmosphere glovebox, a 250 mL round-bottom flask was loaded with (*R*)-[($C_{20}H_{12}O_2$)Si(C_5H_2-2-$SiMe_3$-4-CMe_3)$_2$]-K_2 (6.41 g, 8.27 mmol) and $ScCl_3(THF)_3$ (3.04 g, 8.27 mmol). The reaction flask was attached to a medium-porosity swivel frit equipped with another 250 mL flask and a 90° needle valve adapter. THF (200 mL) was condensed into the flask at −78 °C, and the mixture was refluxed for 48 h. The solvent was removed at reduced pressure, and the resulting yellowish foam was dried at 70 °C under vacuum overnight. Toluene (150 mL) was then added by vacuum transfer, and the mixture was refluxed for 12 h, during which time, small amounts (ca. 5 mL) of solvent were periodically evaporated. The solvent was then completely removed *in vacuo* while the heating oil bath was maintained at 120 °C. The yellow residue was dried under vacuum at 120 °C for 4 h. Diethyl ether (150 mL) was condensed in, and the suspension was stirred at room temperature for 1 h. The solution was filtered, and the white precipitate was washed twice with Et_2O. Evaporation of solvent from the supernatant afforded a yellow foam which was dried *in vacuo* at 70 °C for 6 h. In the glovebox, the foam was crushed into a finely divided solid, and the reaction flask was connected to a new swivel frit assembly. Hexane (100 mL) was transferred onto the solid at −78 °C. The mixture was warmed to room temperature and was vigorously stirred, giving a yellow solution with a white precipitate. The solid was filtered, washed twice with fresh pentane, and dried under vacuum (3.21 g, 50% yield). Anal. Calcd for $C_{44}H_{52}ClO_2ScSi_3$: C, 67.97; H, 6.74. Found: (with added V_2O_5): C, 61.11; H, 7.13. Found (without added V_2O_5): C, 60.91; H, 7.04. Molecular weight by Signer's method: 1638 (benzene). ^{1}H NMR (25 °C, THF-d_8): δ 7.94 (d, $C_{20}H_{12}O_2Si$, 1H, J = 8.7 Hz), 7.87 (d, $C_{20}H_{12}O_2$, 1H, J = 8.2 Hz), 7.66 (d, $C_{20}H_{12}O_2$, 1H, J = 8.8 Hz), 7.30, 7.19, 7.14 (m, $C_{20}H_{12}O_2$, 3H), 6.54, 6.42 (AB spin system, C_5H_2, 2H, J = 2.0 Hz), 1.31 (s, CMe_3, 9H), 0.21 (s, $SiMe_3$, 9H).

Preparation of (*R,S*)-($C_{20}H_{12}O_2$)Si(η^5-2-$SiMe_3$-4-CMe_3-C_5H_2)$_2$Sc(η^3-C_3H_5) (7). In an inert-atmosphere glovebox, a 150 mL round-bottom flask was charged with (*R,S*)-($C_{20}H_{12}O_2$)Si-(η^5-2-$SiMe_3$-4-CMe_3-C_5H_2)$_2$ScCl (0.560 g, 0.72 mmol) and connected to a swivel frit assembly. Toluene (80 mL) was added by vacuum transfer at −78 °C. Under an argon flush, a 1.0 M solution of allylmagnesium bromide (Et_2O, 0.72 mL, 0.72 mmol) was slowly syringed into the stirred solution, maintained at −78 °C. The mixture was warmed slowly to room temperature with stirring overnight, at which time the solvent was removed *in vacuo*. The residue was then treated with *n*-hexane (100 mL); this mixture was stirred, allowed to settle, and then filtered. After the precipitate was washed twice with *n*-hexane, the solvent was removed from the supernatat, affording an orange-red solid (0.450 g, 80%). Anal. Calcd for $C_{47}H_{57}O_2ScSi_3$: C, 72.08; H, 7.34. Found (with added V_2O_5): C, 67.79; H, 7.58. Found (without added V_2O_5): C, 69.65; H, 8.03. ^{1}H NMR (25 °C, toluene-d_8): δ 7.80 (m, CH_2CHCH_2, 1H), 7.67 (d, $C_{20}H_{12}O_2$, 2H, J = 8.8 Hz), 7.58 (d, $C_{20}H_{12}O_2$, 2H, J = 8.8 Hz), 7.54 (d, $C_{20}H_{12}O_2$, 2H, J = 8.0 Hz), 7.36 (d, $C_{20}H_{12}O_2$, 2H, J = 8.6 Hz), 7.09 (m, 2H, $C_{20}H_{12}O_2$), 6.90 (m, 2H, $C_{20}H_{12}O_2$), 7.49 (s (br), C_5H_2, 2H), 6.45 (s (br), C_5H_2, 2H), 5.04 (d (br), *anti*-CH_2CHCH_2, 1H), 4.18 (d (br), *anti*-CH_2CHCH_2, 1H), 2.45 (d (br), *syn*-CH_2CHCH_2, 1H), 2.24 (d (br), *syn*-CH_2CHCH_2, 1H), 1.35 (s (br), CMe_3, 18H), 0.14 (s (br), $SiMe_3$, 18H).

Structure Determination for *rac*-$Me_2Si[\eta^5$-2,4-$(CHMe_2)_2$-$C_5H_2]_2Sc(\eta^3$-$C_3H_5)$ (6). A fragment cut from a single crystal of **6** under Paratone oil was attached to a glass fiber and centered on an Enraf-Nonius CAD-4 diffractometer under a stream of cold N_2 gas. Unit cell parameters and an orientation matrix were obtained by a least-squares calculation based on the setting angles of 25 reflections with 12.5° < θ < 13.3°. During the data collection, three reference reflections were measured every 1 h and showed no significant decay. Two equivalent data sets were collected, and no correction was made for decay or absorption. Lorentz and polarization factors were applied, and the two data sets were then merged in point group 2/*m*. Details of the data collection and solution and refinement of the structure can be found in Table 1. The structure was solved by direct methods, which revealed all non-hydrogen atom positions (SHELXS). Subsequent difference Fourier maps were successful in finding all hydrogens, including hydrogens for both the major and minor allyl sites. In the refinement, the methyl group C−H angles were constrained to 109.5° and the C−H distances for each methyl were allowed to vary as a group; all other hydrogens were unrestrained, including those for both the major and minor allyl sites. All non-hydrogen atoms were refined anisotropically. Full-matrix least-squares refinement on F^2 converged at R_F = 0.0475 and GOF(F^2) = 2.153. The final difference Fourier map did not reveal any significant features. Disorder in the allyl ligand was modeled as a 70/30 distribution of populations using identical methylene carbons and two separate methine carbons. Crystallographic data have been deposited at the CCDC, 12 Union Road, Cambridge CB2 1EZ, U.K., and copies can be obtained on request, free of charge, by quoting the publication citation and the deposition number 113326.

Variable-Temperature ^{1}H NMR Experiments. Samples of the allyl complexes used for variable-temperature ^{1}H NMR studies were washed once with 0.1 mL of the appropriate deuterated NMR solvent, and this solvent was removed *in vacuo*, to ensure the complete removal of trace amounts of solvent from workup of prior preparative scale reactions. Samples were brought to the indicated probe temperature (allowed to equilibrate for 7−10 min), and spectra were accumulated using 16−32 scans and 2−4 s recycle delays. Probe temperatures were calibrated using methanol (low temperature) and ethylene glycol (high temperature) samples as references.

Acknowledgment. This work has been supported by the USDOE Office of Basic Energy Sciences (Grant No. DE-FG03-85ER13431) and by Exxon Chemicals America.

Supporting Information Available: TELP drawings showing the complete atom-labeling schemes, cell and crystal packing diagrams, and tables of atomic coordinates, complete bond distances and angles, and anisotropic displacement parameters for complex **6** and figures giving ^{1}H NMR data for **2**, $Me_2Si\{3$-$[2$-$(2$-Me$)$-$C_{10}H_4]$-$C_5H_3\}_2Li_2$, *meso*-$Me_2Si\{\eta^5$-3-$[2$-$(2$-Me$)$-$C_{10}H_{14}]$-$C_5H_3\}_2ScCl\cdot LiCl(THF)_2$, *meso*-$Me_2Si\{\eta^5$-$3$-$[2$-$(2$-Me$)$-$C_{10}H_{14}]$-$C_5H_3\}_2YCl\cdot LiCl(solv)_2$, **4**, **5**, (*R,S*)-($C_{20}H_{12}O_2$)Si(η^5-2-$SiMe_3$-4-$CMe_3C_5H_2)_2ScCl$, and **7**. This material is available free of charge via the Internet at http://pubs.acs.org.

OM980893S